

THESIS



This is to certify that the
thesis entitled
APPLICABILITY OF THE LORENTZ-OSCILLATOR MODEL
TO INFRARED ABSORPTION IN LITHIUM FLUORIDE

presented by

CHARLES M. RANDALL

has been accepted towards fulfillment
of the requirements for

Ph. D. degree in PHYSICS


Major professor

Date November 19, 1964

ABSTRACT

APPLICABILITY OF THE LORENTZ-OSCILLATOR MODEL TO INFRARED ABSORPTION IN LITHIUM FLUORIDE

by Charles M. Randall

The Lorentz model of a dispersion oscillator with a constant damping factor has long been used to describe the absorption of electromagnetic radiation by a crystal lattice. Modern theoretical investigations indicate that the damping constant should actually vary with frequency. Nevertheless, if the damping factor does not vary too rapidly in the region of the principal absorption, the model remains useful. We have devised a method to obtain the dispersion frequency ω_0 and damping factor γ from the experimental data by a least-squares fitting technique. We have compared the experimental results obtained from thin-film transmission measurements on lithium fluoride with the predictions of theory when isotopic mass, film thickness, and temperature are changed. The agreement is satisfactory for isotopically pure films, and suggests that the method may be useful in characterizing the behavior of isotopically mixed films.

APPLICABILITY OF THE LORENTZ-OSCILLATOR MODEL
TO INFRARED ABSORPTION IN LITHIUM FLUORIDE

By,
Charles M. Randall

A THESIS

Submitted to
Michigan State University
in partial fulfillment of the requirements
for the degree of

DOCTOR OF PHILOSOPHY

Department of Physics and Astronomy

1964

ACKNOWLEDGMENTS

Worthwhile accomplishments are seldom made without the help of many people. It is my privilege to acknowledge those who have made this work possible:

Professor D. J. Montgomery not only suggested and directed the work but has been a constant source of encouragement and counsel. The breadth and depth of his knowledge has been of great help and will always challenge me, while his example in human relations will ever serve as a model.

Dr. John R. Hardy gave several ideas valuable in the interpretation of the data.

The Physics Department shop under the direction of Mr. Richard Hoskins has furnished several pieces of apparatus and much helpful technical advice. In particular Mr. Robert Cochrane carefully constructed several important pieces of equipment.

Richard Fuller and Sitaram Jaswal, fellow graduate students, made many helpful suggestions, provided a sounding board for many ideas, assisted in carrying out the details of many experiments, and helped in many other ways to make this project a success.

The drawings were done carefully and skillfully by Dipak Bāzaj.

Several undergraduates have also been active with the work: Kwok Fai Yeung, who spent hours polishing crystals and helped develop a method of analyzing spectra; Gene Gardner, who has spent many tedious hours transferring spectra from film to cards; and Karl Zetterholm, who took over much of the computer programing and organization of data for analysis.

The MSU Computer Laboratory gave valuable assistance in programing. The high-energy nuclear-physics group under the leadership of Mr. Ronald Beery made the Hydell machine available, and gave several suggestions on computer programing.

The research has been supported by the Air Force Office of Scientific Research and All University Research Grants. I am very grateful to the National Science Foundation for support through a Cooperative Graduate Fellowship.

Last but most important my wife, Bernadette, has been understanding and a source of encouragement during the course of the work, and has given invaluable assistance in the preparation of this thesis, including typing several rough drafts before typing the final form.

To all these people, and to many others who have helped in one way or another, it is my privilege to express my appreciation.

TABLE OF CONTENTS

CHAPTER	Page
I. INTRODUCTION	1
II. APPARATUS AND EXPERIMENTAL TECHNIQUE	3
Sample Preparation	3
Temperature Measurement and Control	5
Thermometer Fabrication	5
Thermometer Calibration	11
Dewar and Temperature Control	12
Transmission Measurements	21
Spectral Analysis	25
III. RESULTS AND DISCUSSION	36
Infrared Dispersion Frequency ω_0	38
Dependence on Thickness	38
Dependence on Isotopic Mass	42
Dependence on Temperature	42
Apparent Thickness d	44
Dependence on Temperature	44
Dependence on Actual Thickness and Isotopic Mass	44
Reduced Damping Constant γ/ω_0	44
Dependence on Actual Thickness	44
Dependence on Isotopic Mass	47
Dependence on Temperature	47
Effect of Isotopic Mixing	50
REFERENCES	54
APPENDIXES	56

LIST OF TABLES

TABLE	Page
I. Supplier's isotopic and chemical analysis of lithium samples	6
II. Expected dependence of single dispersion-oscillator parameters on experimental variables	39
III. Contributions to the temperature dependence of the dispersion frequency of lithium fluoride	45

LIST OF FIGURES

FIGURE	Page
1. Horizontal evaporation arrangement for LiF	4
2. Resistance thermometer and evaporation jig	8
3. Vertical evaporation arrangement for indium	10
4. Indium resistance-thermometer calibration curve	13
5. Low-temperature dewar	14
6. Detail view of dewar tail	16
7. Sample holder	18
8. Resistance-thermometer measuring circuit	19
9. Optical path of spectrophotometer	23
10. Stray-light curve	26
11. Corrected Li ⁷ F spectrum	27
12. Original Li ⁷ F spectrophotometer trace	28
13. Spectrophotometer 100% line	29
14. Corrected and calculated Li ⁶ F spectrum	37
15. Dependence of ω_{\min} on thickness	40
16. Dependence of ω_0 on thickness for Li ⁷ F films	41
17. Dependence of ω_0 on temperature for LiF	43
18. Dependence of apparent thickness on temperature for LiF	46
19. Dependence of γ/ω_0 on thickness for Li ⁷ F films	48
20. Dependence of γ/ω_0 on temperature for LiF	49
21. Theoretical phonon distribution function for LiF	51

LIST OF APPENDIXES

APPENDIX	Page
A. Infrared parameters of a Li^6F film at various temperatures	57
B. Infrared parameters of isotopically-mixed LiF film at various temperatures	58
C. Infrared parameters of a Li^7F film at various temperatures	59
D. Infrared parameters of a series of Li^7F films of various thickness at room temperature	60

CHAPTER I

INTRODUCTION

In 1665 Sir Isaac Newton decomposed white light from the sun into the visible spectrum; in 1800 Sir William Herschel found that the greatest heating power of the spectrum lay outside the visible, just below the red end of the spectrum. Interest in this "infrared radiation" has continually grown as it has been realized that the electromagnetic interactions of the more massive constituents of matter are characterized by it. Every material body emits, absorbs, transmits, and reflects infrared radiation in a characteristic manner. The physicist can and indeed has employed the analysis of this radiation to increase his understanding of both the radiation field and the properties of matter. Technological applications of the radiation and commercial instruments for its study, however, have appeared for the most part only during the last two decades or so.

Our understanding of the interaction of electromagnetic radiation with solids is far from satisfactory. For even the simplest types of solid there has been no theoretical treatment of any rigor, and there has been no experimental study of any completeness. Even with the theoretical models available, until the recent widespread availability of high-speed electronic computers, investigators in this field were forced by the sheer magnitude of the computations involved to make drastic simplifying assumptions. In our laboratory we undertook a program of experimental and theoretical investigation that we hoped could contribute to advancing the understanding of the interaction between the radiation and the vibrations of the crystal lattice in the region where photon energies are comparable with phonon energies, and in materials where the interaction is strong. Thus we were led--as were Czerny¹ and his school in their pioneering work begun 30 years ago--to infrared studies of ionic crystals. We chose substances as simple and familiar as possible, namely the alkali halides, or certain other substances with NaCl structure, and we chose as parameters the

temperature, and wherever it was feasible and worth while, isotopic composition. We chose to study the photon-phonon interaction by means of transmission measurements, since certain parameters describing the phonons are nearly directly evident from this type of data, and since samples are frequently easy to prepare. As is common in scientific work, the apparent simplicity of the infrared response of these materials disappeared upon closer examination. It has become clear that successful quantitative description of the photon-phonon interaction will require extensive data on a full set of materials over a wide range of carefully controlled parameters.

We wish to begin with a substance which is tractable and familiar, and which lets us vary isotopic mass significantly. Lithium fluoride, readily available with Li^6 or Li^7 in proportions as desired in combination with the isotopically pure F^{19} , forms stable and durable films. The binding forces are large enough and the reduced mass of LiF small enough, moreover, to cause the lattice vibration frequencies to be sufficiently great that most of the phenomena of interest lie in regions of the spectrum that are easily investigated with modern commercial infrared spectrophotometers. Techniques for obtaining suitable samples for infrared transmission measurements by evaporation in high vacuum have been developed in our laboratory as well as in others. Largely ignored in other thin-film investigations, however, is careful attention to the problem of temperature measurement and control, which has been in part the object of the present study.

Thin-film measurements can give only part of the information about the photon-phonon interaction, but they give that information in fairly convenient form. In this study we begin the investigation of the limits of the accuracy and the meaning of parameters (infrared dispersion frequency, damping constant, apparent film thickness) as obtained in our thin-film studies. We find that these parameters can be used meaningfully to characterize the observed phenomena in the case of isotopically-pure substances. We then attempt to apply this simple characterization to absorption in isotopically-mixed substances, a much more complicated phenomenon for which experimental results are sorely needed to guide the theory.

CHAPTER II

APPARATUS AND EXPERIMENTAL TECHNIQUE

For convenience we discuss the experimental work involved in this study in four sections; 1) sample preparation, 2) temperature measurement and control, 3) transmission measurements, and 4) spectral analysis.

Sample Preparation

Because of the strong absorption of the alkali halides near their infrared dispersion frequency, transmission measurements in this region must be made on very thin samples, which are conveniently obtained by high-vacuum evaporation onto suitable substrates. The commercial evaporation system used in this study is equipped with a nickel-plated steel base plate through which pass feed-throughs for high currents and for mechanical motion. The pumping system consists of a 4" oil diffusion pump rated at 750 liters per second at 0.1 micron, backed by a 15-cfm mechanical pump. Between the diffusion pump and the base plate is a chevron-type liquid-nitrogen baffle and a 4" gate valve. An ionization gauge is connected to the pumping line just below the base plate. Thermocouple gauges in the high-vacuum line and the forepump line indicate the pressure during roughing operations. The Pyrex bell jar is 14" in diameter and 15 3/8" in height. Usually the system will pump down to the 10 μ Torr region in 4 or 5 minutes, and to less than 5 μ Torr within 30 minutes. Currents up to 250 amps are supplied from a low-voltage transformer connected to the 110-volt lines through a 15-amp variable autotransformer. One of the high-current leads passes through an instrument transformer for monitoring the current through the boat.

The LiF films were evaporated over indium resistance-thermometer elements (to be described later) that had been previously evaporated on the 0.040"-thick high-density polyethylene (HDP) substrates. The horizontal evaporation apparatus used for the LiF films is shown in figure 1. The molybdenum boat was packed with the desired sample material and placed in the evaporator. When the pressure was below 5 μ Torr, the current through the boat was increased over a period of three or four

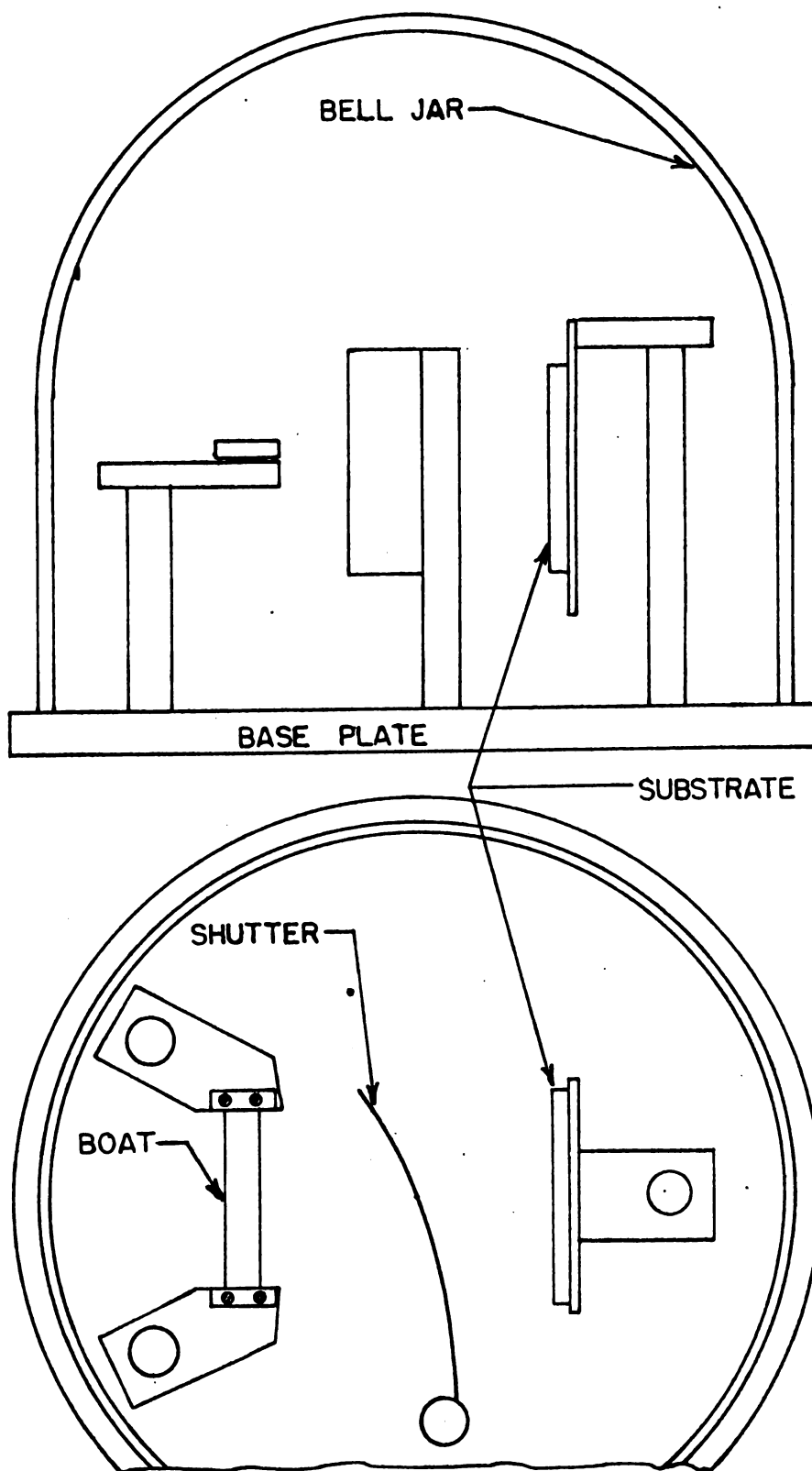


Figure 1. Arrangement for horizontal evaporation of LiF films.

minutes until the boat appeared dull red at typically 200 amperes. The pressure was observed to rise rapidly by several μ Torr and then to fall, probably due to the release of water vapor trapped in the powdered LiF. After the pressure fell to nearly its former value the boat was rapidly heated to bright red and the shutter opened. Experience had shown that a film of suitable thickness appeared green by interference when viewed at nearly grazing incidence in white light reflected from the baseplate. After such a film was produced in from 30 to 50 seconds by a boat about 95 mm from the substrate, the shutter was closed, and the current turned off. The film was then removed from the evaporator and placed in the sample holder prior to insertion in the dewar.

Early runs were made with commercial LiF, for which analysis is unavailable. Later runs were made with isotopically enriched LiF from Oak Ridge National Laboratories. The supplier's isotopic and chemical analyses of the lithium in the three ORNL samples are given in Table I. The samples from which the isotopically mixed films were evaporated were weighed from the ORNL LiF samples on a single-pan balance sensitive to 0.1 mg. Typically 400 mg of a mixture were prepared. Different boats were used for evaporation of films with different isotopic composition.

Temperature Measurement and Control

Inasmuch as the thin films which are under study are deposited on thick substrates, care must be taken to determine the temperature of the film, rather than that of the substrate. Because we are concerned with the average temperature over the area of the film illuminated by the beam of the spectrophotometer, we chose a wide-area resistance thermometer. Very pure indium, whose resistivity changes significantly with temperature down to its superconducting transition at 3.4°K , makes a suitable element².

Thermometer fabrication: - The resistance thermometer is an evaporated U-shaped film of indium in a four-terminal resistor configuration, as shown in the upper part of figure 2. Four small wire stationers staples were punched through the HDP substrate and clinched before the film was evaporated. With ordinary tin-lead radio solder, No. 34 formvar-insulated copper leads were soldered to one end of each staple on the side opposite the side which was to receive the film. With a small soldering iron at about 170°C , a groove was formed in the film side of the HDP from each staple to the anticipated location of its connection with the indium film.

Table I. Supplier's Isotopic and Chemical Analyses of the Lithium from Oak Ridge National Laboratories in the Form of LiF.

The chemical analyses are semi-quantitative results and should not be interpreted or construed to be precise quantitative determinations.

Batch number SS5(hy)

Isotopic Analysis (Atomic Percent)

Li^6 95.72 \pm 0.1%

Li^7 4.38 \pm 0.1%

Semi-quantitative Chemical Analysis in Parts per Million

Ag	<1	Cs	<40	Pb	15
Al	20	Cu	10	Rb	<10
Au	<1	Fe	1,000	Si	75
B	10	Hg	<10	Sn	20
Ba	1	K	<10	Sr	2
Bi	<2	Mg	12	Ti	<1
Ca	550	Mn	<10	V	<1
Cd	<2	Mo	<1	W	<40
Co	<2	Na	25	Zn	<100
Cr	3	Ni	10		

Batch number SS5(b)

Isotopic Analysis (Atomic Percent)

Li^6 99.3 \pm 0.2%

Li^7 0.7 \pm 0.1%

Semi-quantitative Chemical Analysis in Percent

Al	<.01	Fe	.05	Pb	<.01
Ba	.01	K	<.01	Sn	<.01
Be	<.001	Mg	.01	Sr	.01
Ca	.25	Mn	<.01	V	<.01
Cr	<.01	Na	.02	Zn	<.25
Cu	.02	Ni	<.01		

Table I (continued)

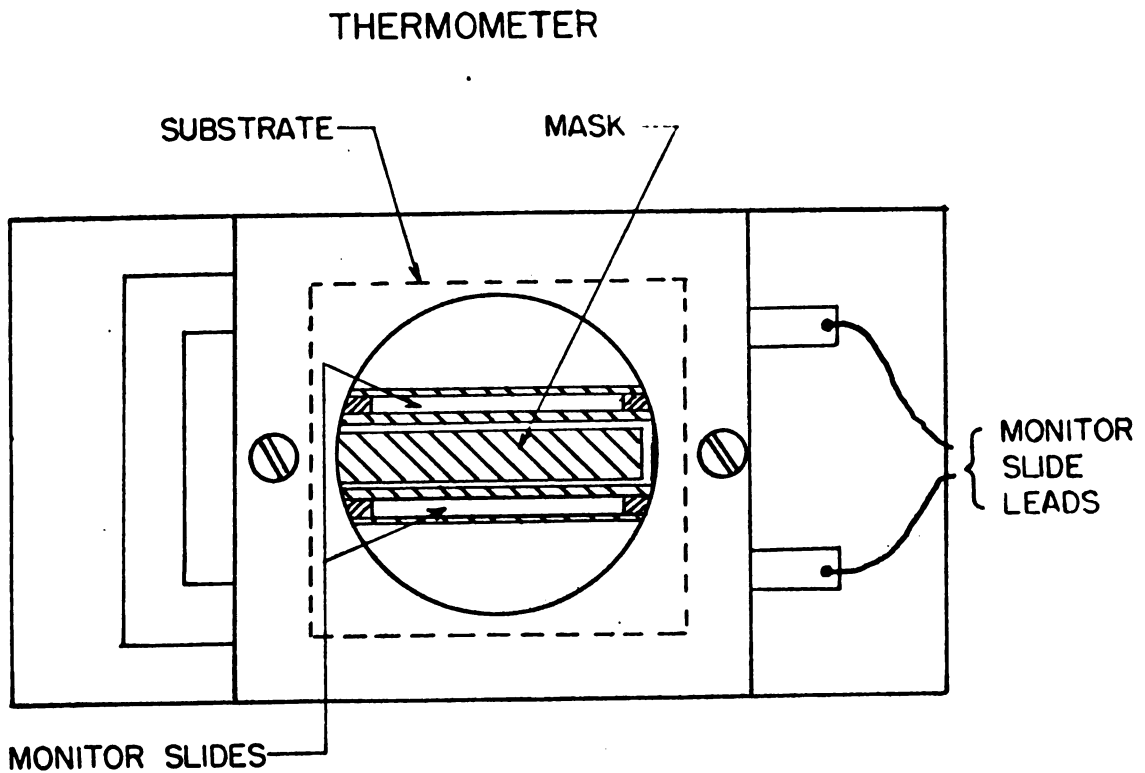
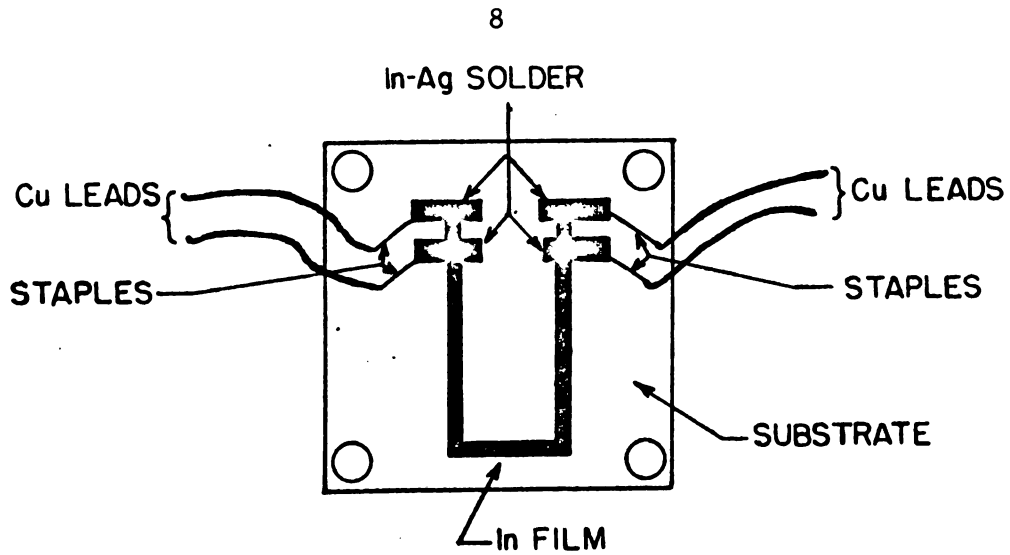
Batch number SS7(c)

Isotopic Analysis (Atomic Percent)

Li⁶ less than 0.01%Li⁷ 99.9924%

Semi-quantitative Chemical Analysis in Percent

Ca	<.004	Fe	.006	Total Metals	<.15
K	<.004	Al	<.001	Carbonate	.06
Na	<.004	Hg	.00938	Total Anions	<.08



EVAPORATION JIG

Figure 2. (Upper) Indium resistance thermometer deposited on a high-density polyethylene (HDP) substrate, showing method of making connections to the film. Not shown is the conducting paint added after the film is evaporated. (Lower) Jig for evaporation of indium film for indium resistance thermometer.

This groove was filled with an indium-silver alloy (95% In-5% Ag) which melts at 165°C , has a wetting ability as high as indium, and greater strength³. The surface of the alloy was made flush with the surface of the HDP by machining and grinding. The resulting substrate was then placed in the evaporation jig shown schematically in the lower part of figure 2. (The HDP has a smooth side and a rough side; it has been found the thermometers are much more reliable if they are deposited on the rough face, possibly because this side seems harder, and has fewer deep scratches that lead to thin spots in the film where early failure may occur.)

The thickness of the thermometer element was estimated during evaporation by noting the resistance of the indium deposited on the fixed geometry of two monitor slides placed beside the mask which controlled the dimensions of the thermometer. These monitor slides were made by using a diamond saw to cut a slot about $1\frac{3}{4}$ " long $\frac{1}{16}$ " away from and parallel to the long side of an ordinary 1" x 3" microscope slide. The central $1\frac{1}{8}$ " portion of the $\frac{1}{16}$ " strip thus formed was temporarily masked with plastic tape, and the ends were covered with a mixture of gold salts in an organic carrier⁴. When the tape was removed and the glass heated to nearly its softening point, the carrier oxidized and left on the glass a conducting gold film, which was then connected to wire leads by pressure contact. The cover which held the slides in place masked them in such a way that the only electrical path between the gold lands was the $\frac{1}{16}$ " glass strip. The two blank monitor resistors, $1\frac{1}{8}$ " x $\frac{1}{16}$ ", were connected in series and their resistance was measured during the evaporation with a laboratory ohmmeter.

The evaporation apparatus is shown schematically in figure 3. Indium of 99.999% purity supplied by the Indium Corporation of America was placed in the molybdenum boat, and the vacuum system was closed and pumped down. Since the presence of oxygen and water vapor in the residual atmosphere of the evaporator will affect the electrical properties of evaporated films⁵, the ratio of water molecules to indium molecules striking the substrate per unit time was lowered by keeping the chevron baffle at liquid-nitrogen temperatures throughout the pumping cycle. The ratio of oxygen atoms to indium atoms was lowered by evaporating indium as a getter over the interior of the bell jar prior to opening

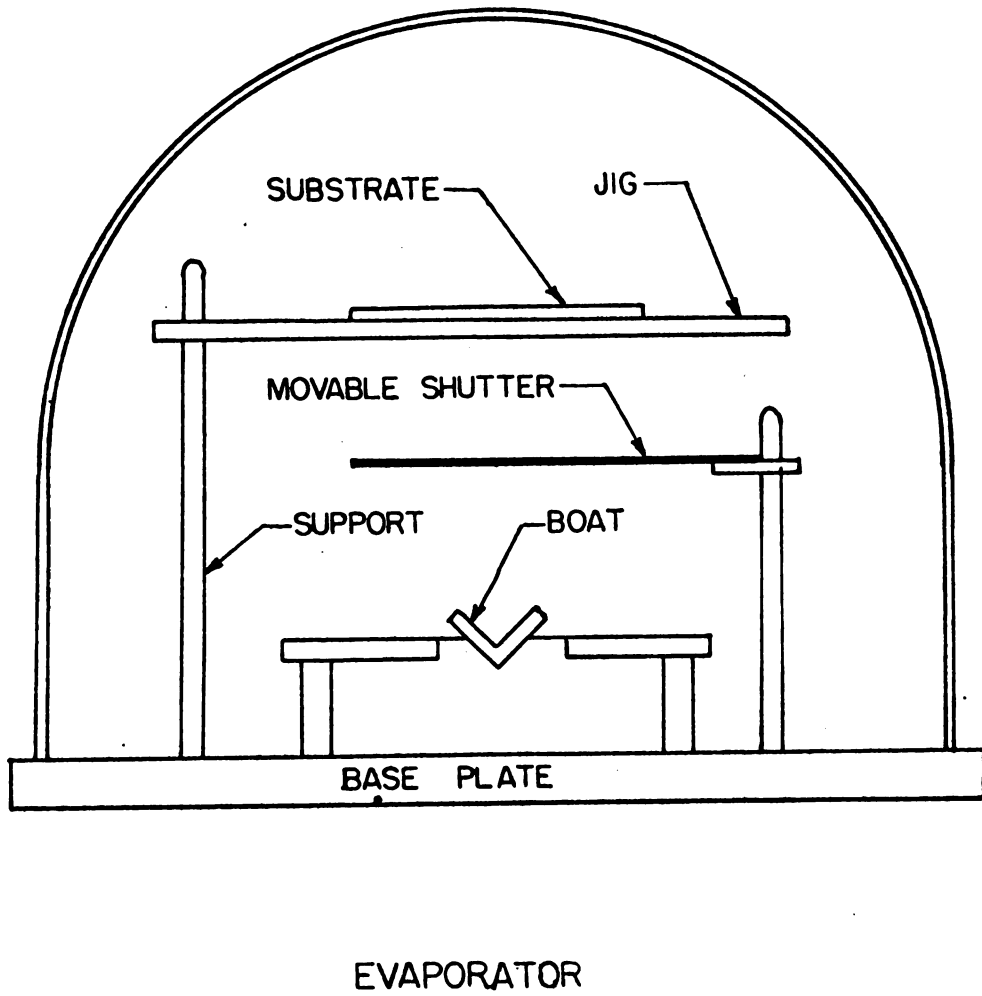


Figure 3. Arrangement for vertical evaporation of indium films.

the shutter between the boat and the evaporation jig to allow the indium film to be deposited on the substrate. The shutter was kept open for 10 to 15 seconds, until the resistance on the monitor slides fell to 8 to 10 ohms, resulting in a thermometer element with a nominal room-temperature resistance of about 20 ohms. When the thermometer was removed from the evaporator, conducting paint was applied between the film and the leads to insure good electrical contact.

Thermometer calibration: - Two thermometers were calibrated by enclosing them in a brass-and-copper container with an electrical heater on the outside. The container was surrounded with sponge-rubber insulation and put inside a brass can about 4" in diameter and 9" long. A copper-constantan thermocouple compared the temperature at the surface of the thermometer with that of the inside surface of the outside brass can. Leads from the thermometer and from the thermocouple were brought out through an 18" length of $\frac{1}{2}$ "-diameter stainless-steel tubing. This tube supported the can and served as a duct for evacuating it with a mechanical forepump, or filling it with helium gas by means of suitable valving.

The current source for calibration consisted of a 1.3-volt mercury battery in series with a 50-ohm precision resistor for measuring the current, and appropriate variable resistors to adjust the current to values not greater than about 1mA. The voltage drop across the resistance thermometer and across the precision resistor, as well as the thermocouple voltage, were measured with a Leeds and Northrup K-3 potentiometer. The thermocouple was also the sensing element for the heater-current controller consisting of a Leeds and Northrup Type-G Speedomax recorder with Double-action Proportional-controller attachment. All the voltages of interest were also continuously monitored with a Daystrom-Weston multipoint recorder.

When the thermometer had been mounted in the can, the system was closed and flushed several times before it was filled to approximately atmospheric pressure with helium as an exchange gas. The can was placed in a stainless-steel dewar, which was then filled with liquid nitrogen. When the system had come to equilibrium as indicated on the recorders, measurements of the various voltages were made with the type-K potentiometer. The resistance R was determined and normalized by dividing by R_0 , the resistance at 0°C . The helium was then pumped out of the can and the

controller set to some temperature and turned on. The measurements were then repeated, after which the controller was set to a new temperature. This cycle was repeated to obtain a complete calibration curve of normalized resistance vs temperature. The curve in figure 4 shows the results of measurements on two films.

Between 0 and 300°K the temperature was determined from the thermocouple voltage by means of preliminary NBS Cryogenic Engineering Laboratory tables which for all temperatures concerned differ by less than a degree from published values⁶. Calibration above 300°K was made with other tables⁷ which for temperatures between 250 and 300°K agree with the cryogenic tables to within ½ degree. A thermocouple, made of wire from the same reel as that for the thermocouple measuring the difference between the can and the thermometer, had one junction attached to the outside of the can and the other immersed in an ice bath. The voltage from this thermocouple was usually from 5.517 to 5.525 mV when the can was submerged in liquid nitrogen. From the tables, this voltage corresponds to a temperature of about 78.5°K, slightly over a degree above the liquid-nitrogen boiling point of 77.4°K. The difference may be due to heat leaks into the can, oxygen dissolved in the liquid nitrogen, or differences between the thermocouples in the present experiment and those used to construct the tables. In any case the temperature is known to within 1 deg-C or about 2% on an absolute basis at liquid-nitrogen temperature, and more accurately at higher temperatures.

Dewar and Temperature control. - The dewar for the optical studies, which was obtained commercially, is shown in figure 5, with details of its lower part shown in figure 6. It is constructed of stainless steel, with the exception of the bottom of the inner tail, and the radiation shields, and the lower part of the outer vacuum container, which are all made of copper or brass. All interior vacuum surfaces are gold plated. The lower mounting ring holds the dewar on an aluminum plate forming the cover of the sample compartment of the spectrophotometer during measurements. The rotating seal allows the substrate to be lined up with either of two pairs of perpendicular openings in the outer vacuum container. Over one pair of openings 0.040"-thick HDP windows are sealed with O-rings. The other pair of openings, which are somewhat larger, will

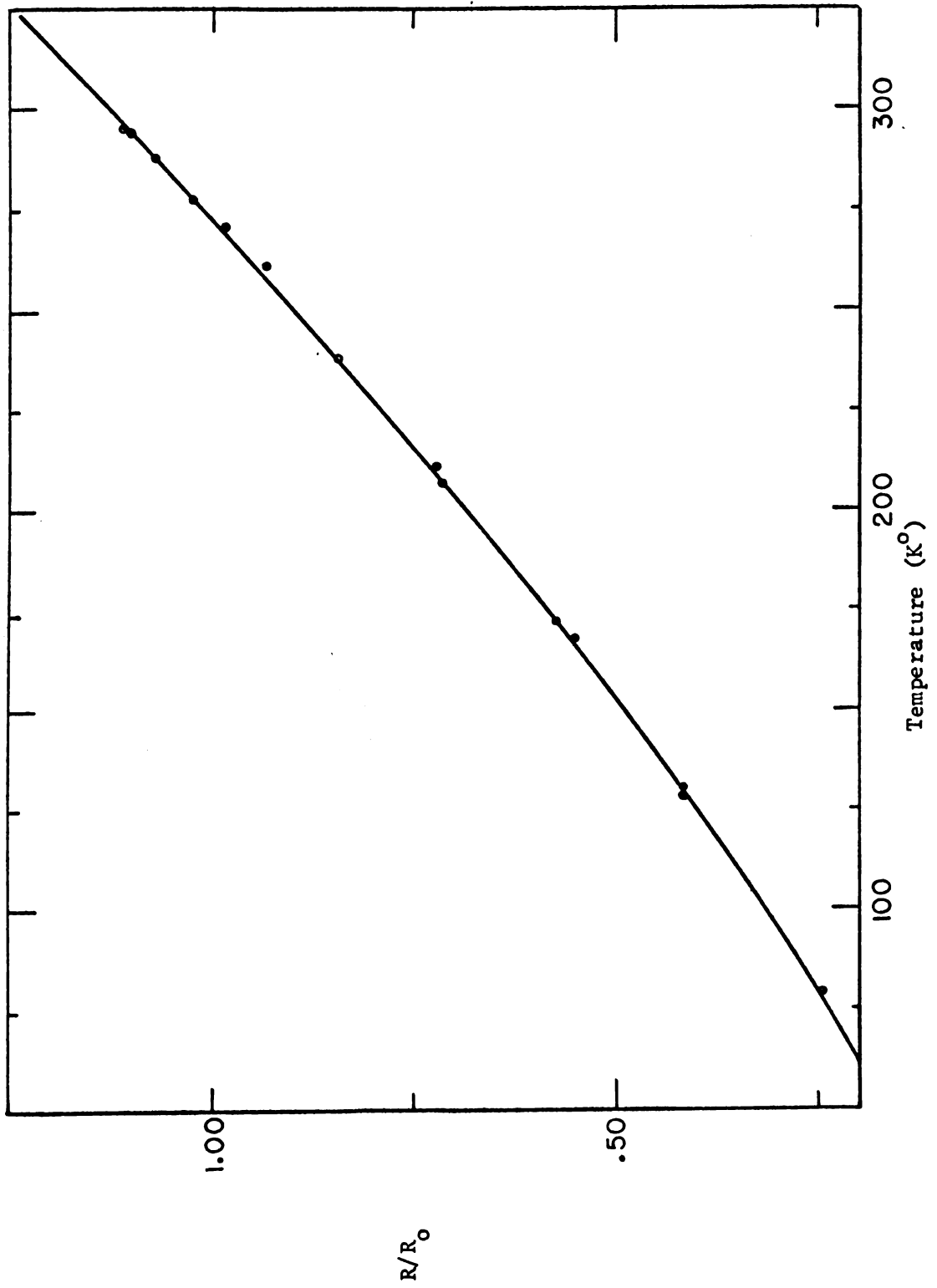
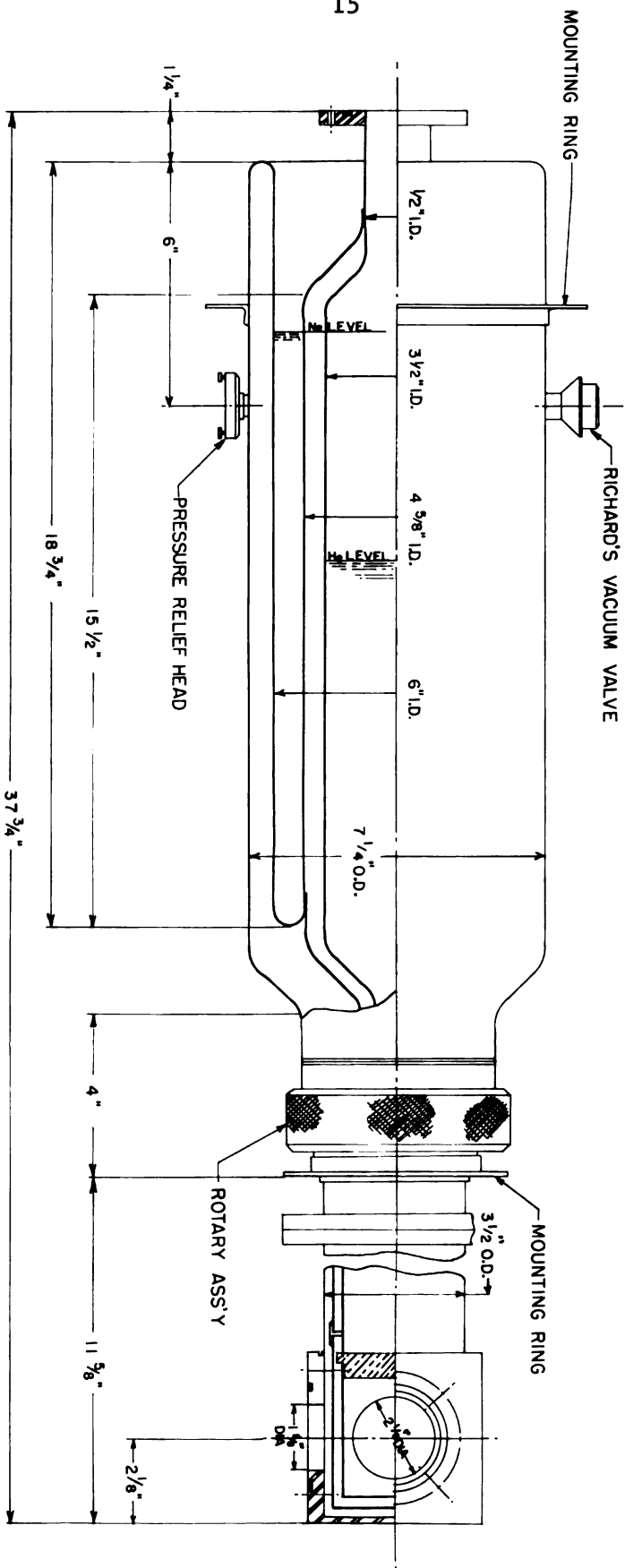


Figure 4. Calibration curve for indium resistance thermometers. Points shown are for two different films.

Figure 5. Dewar used for low-temperature infrared-transmission studies. Not shown are the electrical feedthroughs just above the rotary assembly or in the pressure-relief head.



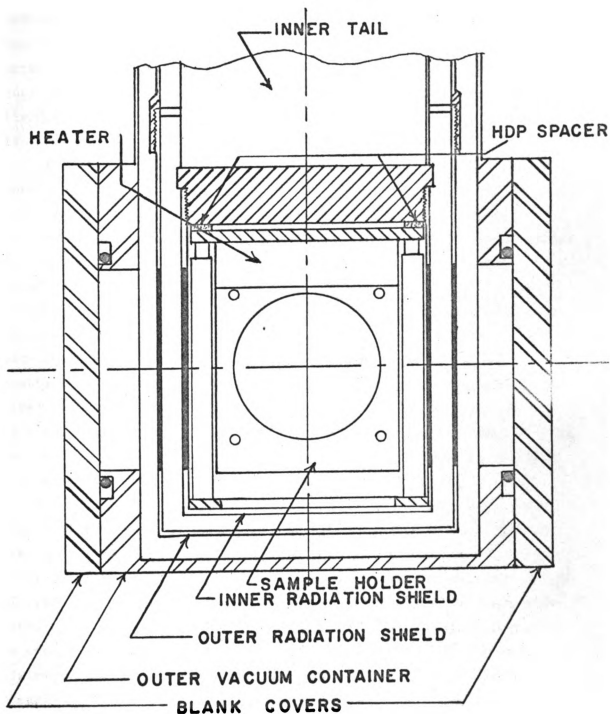
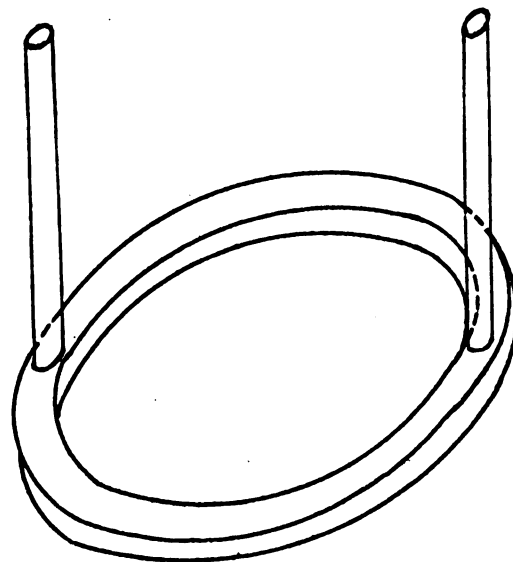
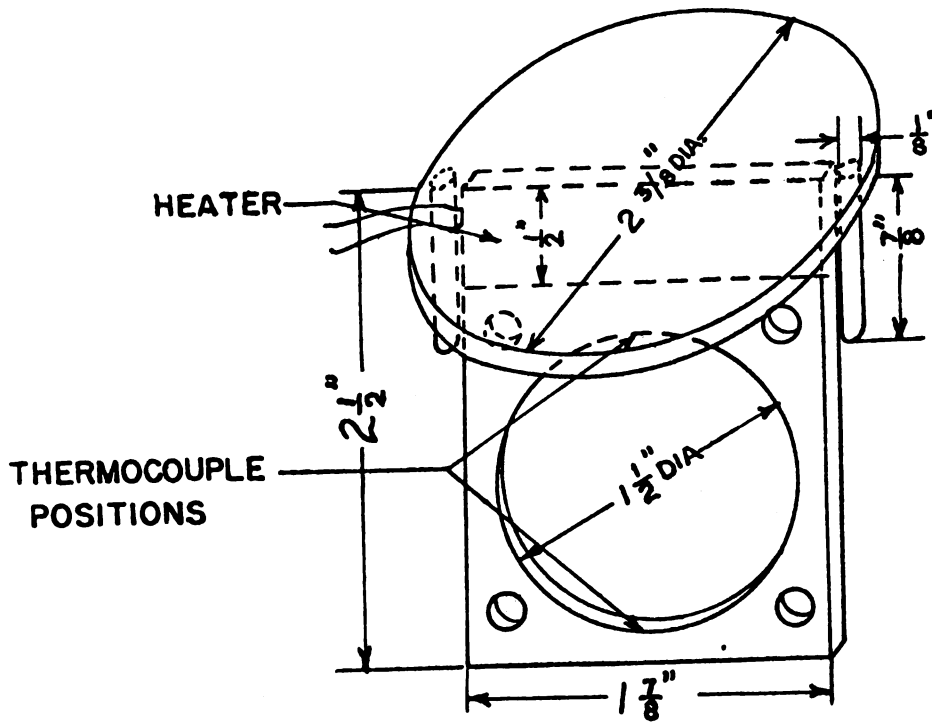


Figure 6. Detail view of the lower portion of the dewar. The two HDP windows in the outer vacuum container through which the infrared radiation passes into the dewar are not shown; they are parallel to the plane of the picture, one in front of, the other behind, the sample holder shown.

eventually be used to evaporate reactive materials within the dewar. They are at present closed with brass plates against O-ring seals. The bottom of the outer radiation shield is attached by a threaded joint in order to facilitate access to the inner tail. The inner radiation shield below the bottom of the inner tail also is screwed on to permit its removal for changing samples.

The sample holder is shown in figure 7. In use the flat copper plate is loaded against the copper block forming the bottom of the inner tail. The leads from the thermocouples, the resistance thermometer, and the heater are brought through holes in the side of the inner radiation shield, and are wrapped around the inner shield for thermal grounding. They are then brought to the outside of the outer shield through holes just above the threaded joint for the bottom part of the outer radiation shield, where they are attached to permanently installed leads which leave the dewar either through feedthroughs just above the rotatable seal, or through a feedthrough installed in the pressure-relief valve. The heater, which consists of two windings of 35 turns of resistance wire connected in parallel, has a resistance of about 45 ohms. The substrate with the indium resistance thermometer carrying the film to be studied is held in place with the film side towards the heavy copper plate by a small plate on the back of the substrate and by four 6-32 machine screws. Two copper-constantan thermocouples are fastened between the small plate and the substrate at the top and bottom of the holder. The junction of one couple is placed at the bottom, and is referred to a junction at the top to give the difference in temperature across the holder. One junction of the other thermocouple is placed at the top of the holder, and is referred to a junction in an ice bath, to give the absolute temperature of the top of the holder. The K-3 potentiometer can be switched to measure any of the thermocouple voltages. In addition these voltages are continuously monitored with the multi-point self-balancing recording potentiometer. Since the potentials of some of the thermocouples may change polarity during the course of a run, the recorder zero is displaced with a simple voltage divider powered by a 1.35-V mercury battery.

The current supply for the resistance thermometer is shown in figure 8. Coarse adjustment of the thermometer current is made by



SAMPLE HOLDER

Figure 7. Copper sample holder. The heater consists of several turns of resistance wire wrapped around the vertical copper block and insulated from it by Teflon tape. The thermocouples are clamped between the HDP substrate and the brass backing plate (not shown).

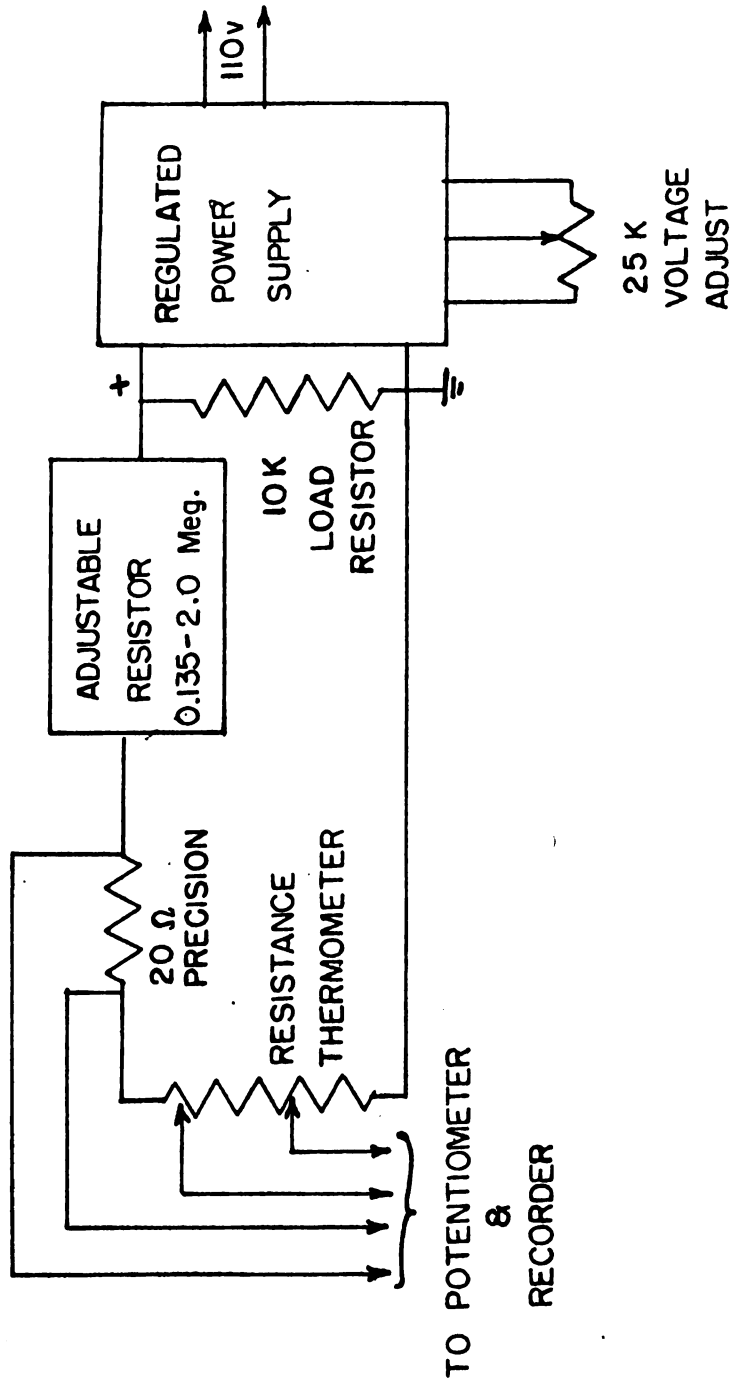


Figure 8. Block diagram of the resistance-thermometer measuring circuit.

switching various fixed dropping resistors into the circuit with the adjustable resistor. Fine adjustment is made by means of a 10-turn potentiometer which varies the output voltage of the Zener-diode-stabilized regulated power supply between 100 and 250 volts. Since the resistance of the thermometer represents only a very small fraction of the total resistance of the load on the power supply, this supply is essentially a constant-current source. The voltage across the thermometer potential terminals is therefore directly proportional to the thermometer resistance. This voltage, as well as the voltage drop across the 20-ohm precision resistor in the current supply, can be connected by a switch to the K-3 potentiometer to permit the resistance of the thermometer to be determined. The voltage across the thermometer is also continuously monitored by the multipoint recorder.

The thermometers under the LiF films were not individually calibrated. They were normalized by assuming that the film and the thermocouple were at the same temperature just after the film was installed in the dewar and before liquid nitrogen had been added. From the normalized resistance expected at this temperature according to the calibration curve (figure 4) and from the measured resistance, a value for the resistance at 0°C , R_0 , was estimated, and used to normalize the resistance values measured subsequently. Because all temperature measurements depend on the first one, temperatures measured with the resistance thermometer are probably not better than about 5%.

As a rough check on the temperature-measuring devices, after measurements were completed on the substrate and thermometer used to obtain 100% lines from the spectrophotometer, the outside vacuum cover and the outer radiation shield were removed from the dewar. Then the inner tail with the sample cell attached was surrounded first by liquid nitrogen and later by ice water. With calibration as described above, the indium film when surrounded by nitrogen (boiling point 77.4°K) indicated a temperature of 76.5°K . The thermocouple first indicated a temperature of 79.8°K , but then slowly drifted up to 84°K . This shift is probably due to thermal gradients across the soldered connections in the thermocouple leads to the sample cell. When the tail was surrounded by ice water, the signal from the thermocouple was zero, indicating the thermal-gradient problems are significant only for large temperature

differences, where they may limit the accuracy of such measurements to about 10%.

The potential from the thermocouple showing the temperature difference between the sample holder and the ice bath, after passing through an RC filter with a time constant of about 4 seconds, forms the sensing signal for the heater controller. The difference between this potential and that from another mercury-battery-powered voltage divider set to deliver a voltage corresponding to the desired temperature, is applied to the input of a Leeds and Northrup DC microvolt amplifier. The output of this amplifier, after further amplification by a Mandrel DC amplifier, becomes the error signal applied to a CD current regulator controlling the heater current⁸.

For most measurements the sample holder was spring loaded against two ring-shaped spacers of 0.040"-thick HDP on the bottom of the inner tail. After evacuation of the dewar, the inner and outer tails were filled with liquid nitrogen. Since the spacers thermally insulate the sample holder, the equilibrium temperature reached in this way was still considerably above liquid-nitrogen temperatures. To decrease the temperature further, the vacuum space of the dewar was filled with helium gas as a heat exchanger. When the temperature had nearly reached its new equilibrium value, the helium was pumped out and measurements were begun. When higher temperatures were desired the heater input power was first adjusted for the maximum that the heater could stand. When the desired temperature was reached, the power was reduced to approximately that needed to maintain the temperature, and the amplified error signal from the thermocouple was fed into the regulator to provide continuous control. With this system it was possible to change to a new temperature and attain equilibrium within an hour. After equilibration the thermocouple potential usually remained constant to within $\pm 30 \mu V$, corresponding to temperature variations less than $\pm 1.5^\circ K$.

Transmission Measurements

The transmission spectra of the LiF films were obtained with a commercial double-beam far-infrared spectrophotometer, the Perkin-Elmer Model 301. A diagram of the optical path of this instrument is shown

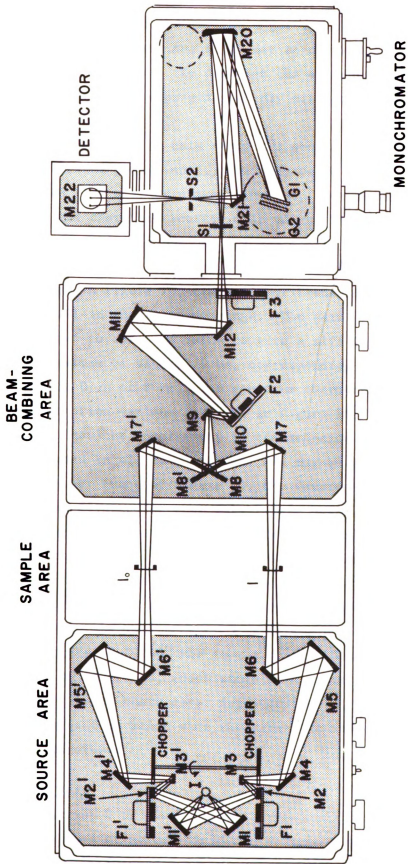
in figure 9. Between the source at I and the Golay detector, several of the reflection elements, the transmission filters at F3 and the crystal choppers, may be changed to isolate a narrow band of the electromagnetic spectrum for dispersion by the grating G1. The mechanical linkage between the grating and its synchronous-drive motor is designed so that the frequency passed by the monochromator is directly proportional to the number of drive-shaft turns, which is presented on an arbitrary scale of 100 "drum turns" per revolution. Calibration of the drum turns in terms of frequency for any grating is made by operating the instrument in the single-beam mode and observing the positions of the atmospheric-absorption bands (mostly due to water vapor). The frequency of these bands is taken from the literature⁹, and a straight line is fitted to the data by the method of least squares.*

The ratio of the signals in the two beams is presented on a visual-readout indicator and on a strip-chart recorder driven by a synchronous motor. The position of a point on the strip chart is correlated with the position of the wavenumber drive by a microswitch operated by a cam on the wavenumber drive. The microswitch actuates a device which marks pips along the edge of the recorder chart or on the pen trace itself. A pip appears for every drum turn number ending in zero, and an extra pip appears for numbers ending in 95.

To keep the instrument from having widely varying sensitivity as it scans through atmospheric-absorption bands, the instrument maintains a constant signal level in the reference beam by adjusting

*After our calibrations were completed a paper¹⁰ appeared which gave a list of more precise values for the atmospheric-absorption lines as found with a Perkin-Elmer 301 instrument. These new values are estimated to be correct to within 0.1 cm^{-1} . The differences between the frequencies assigned in this recent paper and those taken by us for the calibration lines of the 30-line/mm grating used in the study are, with one exception, all less than 0.35 cm^{-1} , the new assignments tending to be about 0.1 cm^{-1} lower than the older ones. The difference is unimportant in studying the rather broad lattice-vibration bands, which have half-widths of about 35 cm^{-1} .

Figure 9. Optical path of the Perkin-Elmer 301 far-infrared spectrophotometer. Reflection elements on F1, F1', and F2 may be changed from outside the instrument. Mirrors M4, M4', and M12 (along with the choppers) may also be changed to isolate a band of the electromagnetic spectrum for dispersion by the grating G1 before detection by the Golay cell near M22.



DOUBLE - BEAM FAR - INFRARED SPECTROPHOTOMETER

the slit width by means of a suitable servo mechanism. The instrument may also be operated with the slits set to a fixed width up to their maximum opening of 10 mm. To decrease the atmospheric absorption, the instrument is constantly purged with dry nitrogen obtained by boiling liquid nitrogen.

For all the work in this study the source was a globar operating at about 200 watts power input. The dispersive element was a 30-line/mm grating, with fine scatter plates (that is, mirrors which appear to be sandblasted and therefore scatter much of the high-frequency radiation) at M2, M4, M2', M4', and M12; an NaF reststrahlen filter at M10; and Kbr choppers. A record of the stray light with this combination of components is given in figure 10, the apparent transmission of a 77-mm thick crystal of NaCl in the relevant range. The gain of the amplifier was always adjusted to the same value to give a slit width at the LiF absorption maximum of about 3.0 mm, corresponding to a spectral slit width of about 0.7μ or 8 cm^{-1} . A spectrum corrected for slit width near the absorption maximum is shown in figure 11. The correction is much smaller than the uncertainty in transmission measurements, and has been ignored in all calculations. As may be seen from the typical spectrophotometer trace of figure 12, the damping in the various servo mechanisms was adjusted so that very little noise is apparent in the recorder trace. The proper amount of damping required the scanning speed to be rather slow in order to keep the tracking error small; consequently the spectra were scanned at the rate of $7.73\text{ cm}^{-1}/\text{min}$ or slower. Spectra of LiF films were always obtained with three thicknesses of 0.040" HDP in the reference beam to compensate for the two windows and the substrate of 0.040" HDP in the dewar. The degree of compensation is exhibited in figure 13, which shows spectra of an HDP substrate with an indium resistance thermometer deposited on it, but without a LiF film. Almost no change took place when the substrate was cooled to liquid-nitrogen temperatures.

Spectral Analysis

The fraction D of electromagnetic radiation of angular frequency, ω , transmitted at normal incidence through a parallel-sided dielectric slab of thickness d is found from Maxwells's equations to be:

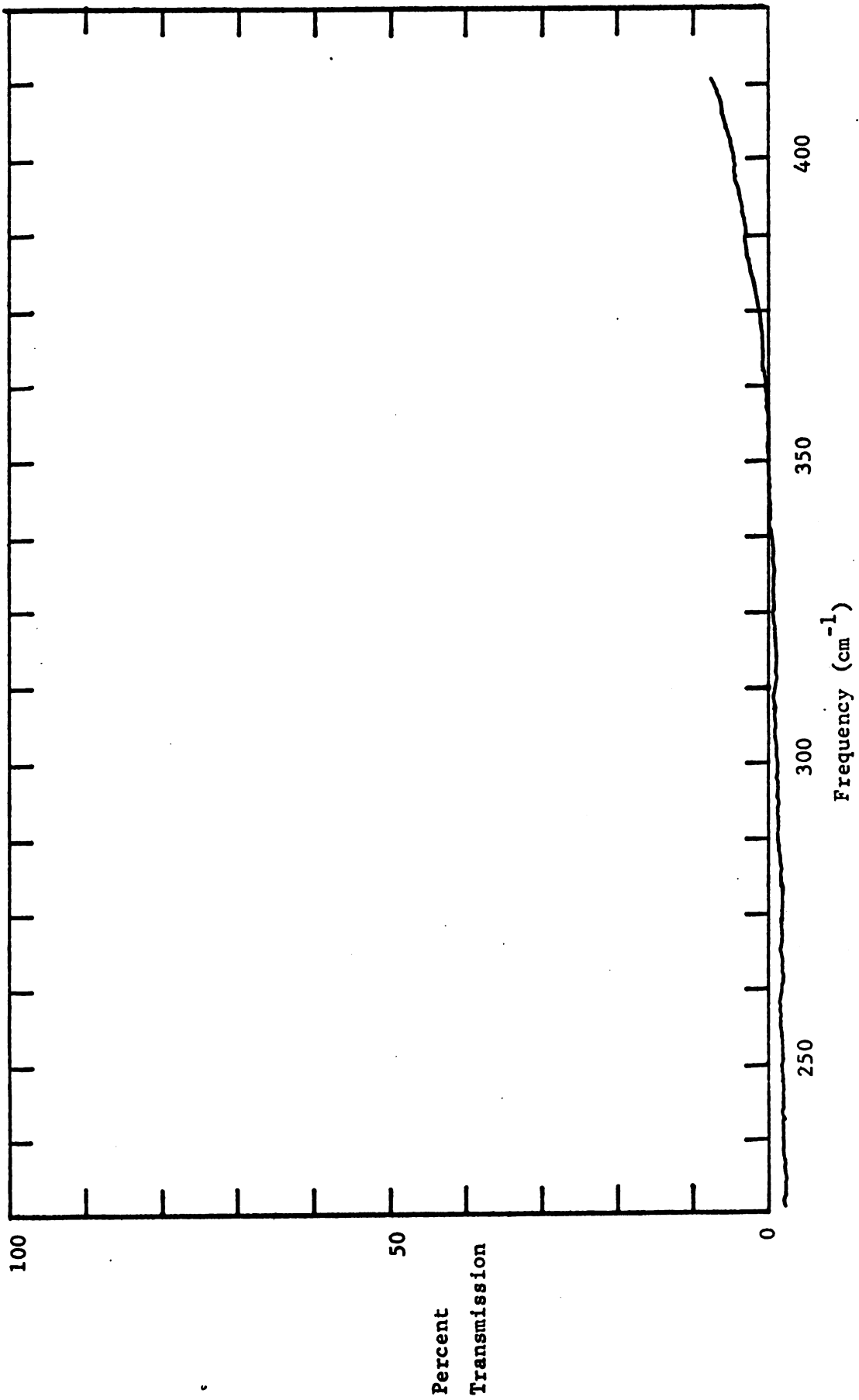


Figure 10. Stray-light curve obtained by recording the apparent transmission of a 77-mm thick crystal of NaCl. Negative transmission values indicate imperfect electrical compensation between the signals from the two beams of the spectro-photometer.

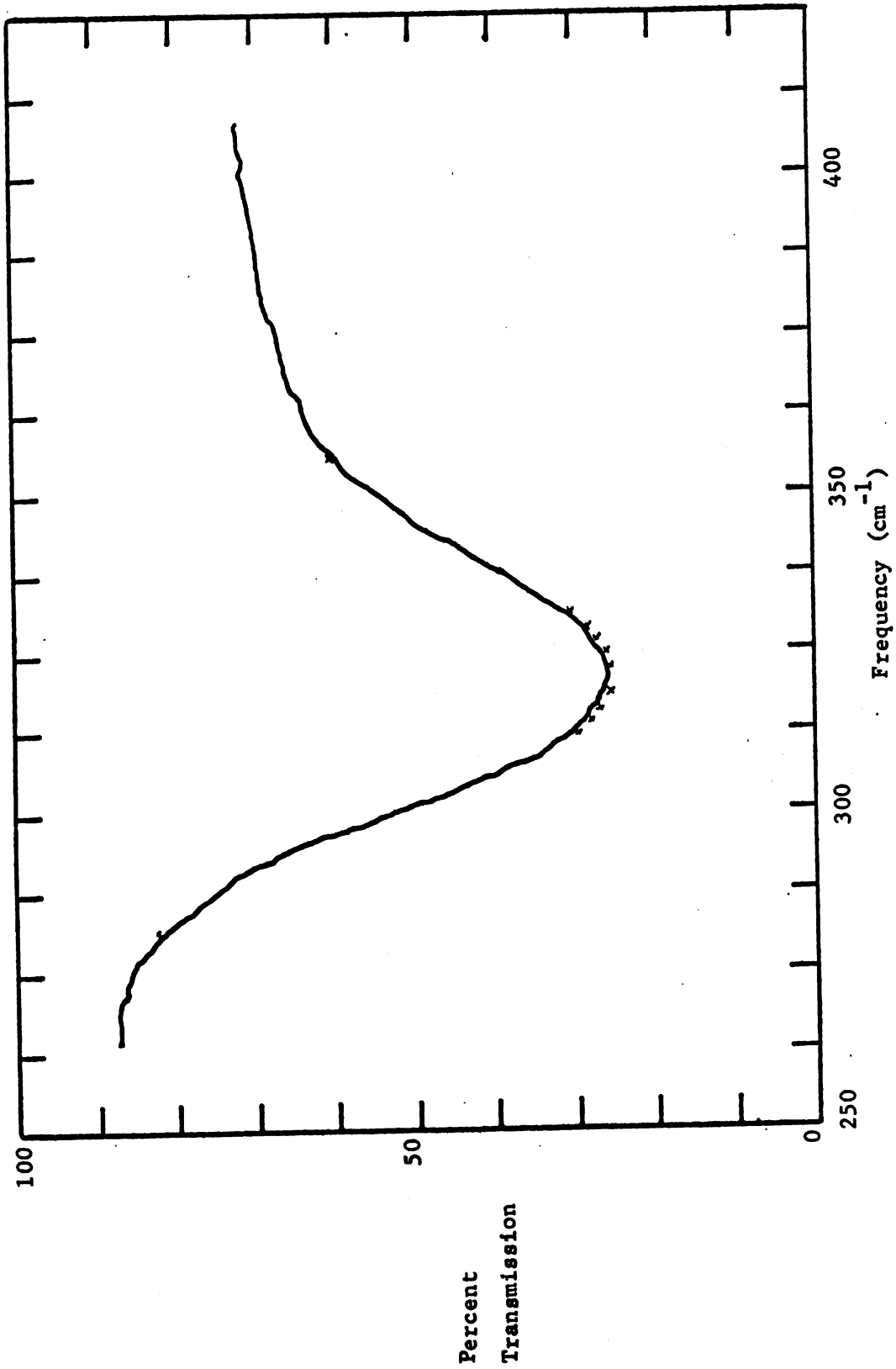


Figure 11. The spectrum of a Li⁷F film at 118°K corrected for changing 100% and 0% lines, as plotted by the computer. The crosses indicate the additional correction for finite width of the slits.

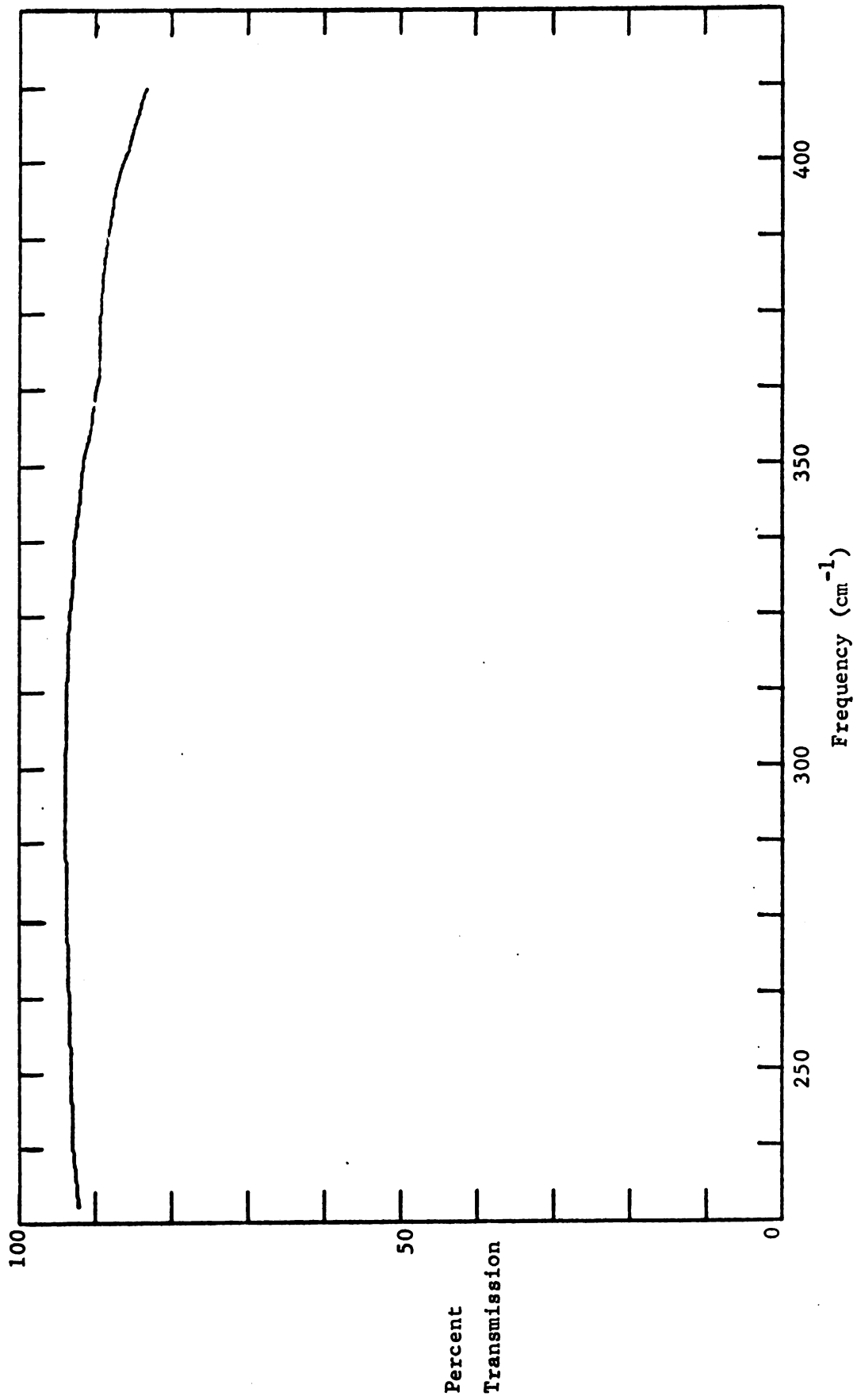


Figure 13. A 100% line as replotted by the computer.

$$D = \left| \frac{4\bar{n} e^{-i\omega d/c}}{(1+\bar{n})^2 e^{-i\bar{n}\omega d/c} - (1-\bar{n})^2 e^{i\bar{n}\omega d/c}} \right|^2 \quad (1)$$

where \bar{n} is the complex index of refraction related to the complex dielectric constant $\epsilon(\omega)$ and the permeability μ by $\bar{n}(\omega) = (\epsilon/\mu)^{1/2} = \epsilon^{1/2}$ for $\mu = 1$. There exists no theories at present which indicate in any detail the form and the temperature dependence of $\epsilon(\omega)$. Hence we chose a basically phenomenological model suggested initially by Lorentz, namely, a single dispersion oscillator of frequency ω_0 and damping constant γ . This model gives the following expression of $\epsilon(\omega)$:¹¹

$$\epsilon(\omega) = \epsilon_\infty + \frac{\epsilon_0 - \epsilon_\infty}{1 - (\omega/\omega_0)^2 - i(\gamma/\omega_0)(\omega/\omega_0)} \quad (2)$$

where ϵ_∞ , the dielectric constant in the visible region of the spectrum, summarizes the effects near ω_0 of vibrations (other than those of the lattice) whose characteristic frequencies are much higher than ω_0 , e.g., polarization of the electron clouds in the atoms; the quantity ϵ_0 , the dielectric constant at frequencies much less than ω_0 , represents the effects of polarization of the entire crystal, including distortion of the ionic cores.

The result of inserting this expression for the dielectric constant in equation (1) is too complicated to yield directly much information about the parameters in equation (2). For thin films equation (1) may be expanded in a series of powers of $\omega d/c$. A suitable approximation is provided by including powers through the second. When equation (2) is used to give \bar{n} , simple expressions for the parameters in equation (2) may be obtained¹² based on data for ω within $\pm 10\%$ of ω_0 :

$$\gamma/\omega_0 = \left\{ \left[1/(D_\infty - D_{\min}) - 1/D_\infty \right] S \right\}^{1/2}, \quad (3a)$$

$$d = \frac{2c}{\omega_0(\epsilon_0 - \epsilon_\infty)} \left[1 - (D_{\min}/D_\infty)^{1/2} \right] \left[S/(D_\infty - D_{\min}) \right]^{1/2}, \quad (3b)$$

$$\omega_0 = (\omega_- \omega_+)^{1/2}. \quad (3c)$$

where ω_- and ω_+ are the frequencies on either side of the transmission minimum which have equal values of transmission, S is the slope of the graph of $(\omega/\omega_0 - \omega_0/\omega)^2$ as a function of $[1/(D_\infty - D) - 1/(D_\infty - D_{\min})]$, D_{\min} is the minimum value of the transmission, and D_∞ is the transmission outside the absorption band and differs from unity as a result of scattering and absorption by other mechanisms. The expressions for d and γ/ω_0 require a tedious plotting to find S . If one picks two special points, however, on the spectrum, one at ω_0 where $D = D_{\min}$, and the other at $\omega_{1/2}$ where $D = \frac{1}{2}(D_\infty + D_{\min})$, still simpler expressions for d and γ/ω_0 result:

$$\gamma/\omega_0 = (D_{\min}/D_\infty)^{1/2} \left| \frac{\omega_{1/2}}{\omega_0} - \frac{\omega_0}{\omega_{1/2}} \right|, \quad (4a)$$

$$d = \frac{2c}{\omega_0(\epsilon_0 - \epsilon_\infty)} \left[1 - (D_{\min}/D_\infty)^{1/2} \right] \left| \frac{\omega_{1/2}}{\omega_0} - \frac{\omega_0}{\omega_{1/2}} \right|. \quad (4b)$$

In the process of getting these convenient expressions, however, we have thrown away not only all the curve with ω differing from ω_0 by more than 10%, but all the curve within this range except for three points at the abscissas ω_0 , $\omega_{+1/2}$, and $\omega_{-1/2}$. The availability of a high-speed computer makes it feasible to extract the parameters directly from a larger portion of the transmission curves by adjusting d , ω_0 , and γ until the $D(\omega)$ curve calculated from equation (2) inserted in equation (1) fits the experimental curve. The criterion

for a best fit is a minimization of the sum of the squared deviations between the calculated and experimental curves. Inasmuch as this nonlinear least-squares method is applicable to a wide range of problems where the parameters in some known analytical function are to be adjusted for a best fit to experimental data, we describe the method in rather general terms¹³.

The function $D(x_i; a_j)$ to be fitted is assumed to have a known analytical form dependent on M independent variables x_i ($i = 1, \dots, M$) and on P adjustable parameters a_j ($j = 1, \dots, P$). A set of N experimental values of D corresponding to N sets of values for the independent variables $x_{i\alpha}$ ($\alpha = 1, \dots, N$) is assumed to be available; and the elements of this set will be labeled $D_{\text{exp}\alpha}$. The value of the D calculated from the known expression for the same set of independent variables will be labeled $D(x_{i\alpha}; a_j)$. The criterion for the best fit is that

$$\sum_{\alpha=1}^N [D(x_{i\alpha}; a_j) - D_{\text{exp}\alpha}]^2$$

be a minimum. This condition will be met when

$$\frac{\partial}{\partial a_k} \sum_{\alpha=1}^N [D(x_{i\alpha}; a_j) - D_{\text{exp}\alpha}]^2 = 2 \sum_{\alpha=1}^N [D(x_{i\alpha}; a_j) - D_{\text{exp}\alpha}] \frac{\partial D}{\partial a_k} = 0$$

($k = 1, \dots, P$). (5)

We expand D in a Taylor series in the a_j about some initially guessed set of a_j 's, denoted a_{j0} , and keep only the first-order terms:

$$D(x_{i\alpha}; a_j) = D(x_{i\alpha}; a_{j0}) + \sum_{m=1}^P \frac{\partial D}{\partial a_m} \bigg|_{\substack{a_{j0} \\ x_{i\alpha}}} \Delta_m$$

To first-order terms, the criterion for best fit then becomes;

$$\sum_{\alpha=1}^N \left\{ D(x_{i\alpha}; a_{j0}) - D_{\text{exp}\alpha} + \sum_{m=1}^P \frac{\partial D}{\partial a_m} \bigg|_{\substack{a_{j0} \\ x_{i\alpha}}} \Delta_m \right\} \frac{\partial D}{\partial a_k} \bigg|_{\substack{a_{j0} \\ x_{i\alpha}}} = 0 \quad (k=1, \dots, P)$$

This equation may be rewritten

$$\sum_{m=1}^P b_{km} \Delta_m = C_k, \quad (k=1, \dots, P) \quad (6)$$

where

$$b_{km} = \sum_{\alpha=1}^N \left. \frac{\partial D}{\partial a_m} \right|_{\substack{a_{j_0} \\ x_{i\alpha}}} \left. \frac{\partial D}{\partial a_k} \right|_{\substack{a_{j_0} \\ x_{i\alpha}}}$$

$$C_k = \sum_{\alpha=1}^N [D(x_{i\alpha}; a_{j_0}) - D_{\text{exp}\alpha}] \left. \frac{\partial D}{\partial a_k} \right|_{\substack{a_{j_0} \\ x_{i\alpha}}}$$

Since the b_{km} and the C_k are calculable from the known form of D , the guessed values for the parameters, and the experimental values for D , the set of P linear equations in P unknowns of equation (6) may then be solved for the Δ_m , which may then be used as a correction to the a_m . The entire process is repeated, each time with $a_{m0}^{(\text{new})} = a_{m0}^{(\text{old})} + \Delta_m$, ($m = 1, \dots, P$) until none of the a_m change significantly from one iteration to the next.

To apply this procedure to finding the parameters for the dispersion oscillator, we take equation (1) with $\epsilon(\omega)$ as given by equation (2) for the function D in the nonlinear least-squares analysis. Only one independent variable occurs, the frequency ω . The adjustable parameters are d , ω_0 , and γ . We have established empirically that the final values of these parameters are essentially independent of the initial guesses put into the analysis, provided these guesses are close enough for the analysis to work at all.

Values of ϵ_0 and ϵ_∞ were not adjusted by the computer analysis, but were taken as constants from the literature¹⁴. Although both constants are temperature dependent, ϵ_0 shows the larger changes owing to the thermal expansion that decreases the number of particles per unit volume and alters the electric fields by changing the distance between particles. In addition there is a small direct effect independent of

volume changes. We estimate that lowering the temperature from 300°K to 100°K lowers ϵ_0 from 9.27 to 8.85¹⁵. Since ϵ_∞ depends primarily on the electron displacements within the ions, its temperature dependence is much weaker, increasing by 0.0072 from its value of 1.92 at 300°K to 1.93 at 100°K¹⁶. We have investigated by direct substitution the effect on the values of d , γ/ω_0 , and ω_0 , as obtained from our analysis of the data, when the dielectric constants are changed by amounts of the same order of magnitude as those due to the maximum temperature change. The largest effect is a change of about 4.5% in the estimated thickness. The change in γ/ω_0 is less than 0.3%, and in ω_0 less than 0.03%. Since these changes are all less than the limit of precision of our measurement and analysis, we have adopted room-temperature values of $\epsilon_0 = 9.27$ and $\epsilon_\infty = 1.92$ throughout our analysis.

The computations required for the analysis outlined are feasible only for a high-speed computer. Hence the analog information from the spectrophotometer must be converted to a digital form acceptable to the computer. For this conversion we photographed the strip-chart record of the desired spectrum on 35-mm High-Contrast Copy Film (Kodak M 135-36) with an Exakta camera equipped with a 58-mm Biotar lens. An exposure of 1/25 seconds at $f/2.8$ to $f/3.5$ was satisfactory with illumination from two 2 x 15-watt fluorescent desk lamps about 14 inches from the paper. After development, the film was projected in a Hydell mobile-stage scanning machine with a Datex-encoder system which punched on IBM 80-column cards the cartesian coordinates (in arbitrary units) of any point on the photograph selected. The course of the transmission curve was traced out with a series of points punched by the Hydell machine. These cards were then used as input data to the computer program written in Fortran 60 for the MSU Control Data 3600 Computer.

The first part of the program read the data cards, checked them for certain errors in format, then converted the cartesian coordinate points from the Hydell machine digitizer to a table of percent transmission as a function of wavenumber. At this point it was possible to subtract point-by-point another spectrum to correct for stray light, and to divide by a third spectrum to correct for any change in the 100% line of the spectrophotometer. The corrected spectrum, along with

certain identifying and control information, was then stored on magnetic tape.

After all the spectra in a particular computer run had been read, scaled, corrected, and stored on tape, the tape was rewound and the spectra were read one by one, and the parameters d , ω_0 , and γ were determined in one of two ways: 1) by means of the nonlinear least-squares method described above applied to the entire spectrum, 2) by means of the nonlinear least-squares method applied to the portion of the spectrum lying within $\pm 10\%$ of the minimum transmission value. The printed output contained in addition to certain identifying information, the values of d , ω_0 , γ/ω_0 , ϵ_0 , and ϵ_∞ , along with estimates of the error in each of the adjusted parameters. It contained also a table of the experimental transmission, the calculated transmission, and the difference between the two transmissions for each wavenumber which happened to be chosen for data punching. If desired the plotter attached to the computer plotted the calculated transmission as a function of wavenumber, and the corrected experimental transmission as a function of wavenumber.

CHAPTER III

RESULTS AND DISCUSSION

A typical absorption spectrum of transmission versus wavenumber is shown in figure 14. Here the dotted line shows the experimentally determined spectrum at 118°K for a Li⁶F film evaporated on HDP, with correction for changing 100% and 0% lines. Modern theory of the absorption indicates that at low temperatures at least, a Lorentzian dispersion oscillator should be a satisfactory model, provided the damping constant is allowed to vary somewhat with frequency. Since the theoretical evaluation of this variation is very difficult, it is necessary to determine it from the experimental results. For our purposes, we wish to examine the feasibility of the approximation of taking the parameters ω_0 and γ/ω_0 as constants, to see whether the function thus obtained fits enough of the curve to render these parameters useful for characterizing the interaction of electromagnetic radiation with crystalline lattices. When the entire observed spectrum shown in figure 14 is used to determine the parameters according to the nonlinear least-squares fit described earlier, the solid line shown is obtained. When only the portion of the spectrum within $\pm 10\%$ of ω_0 is used, the dashed line shown is obtained. The fit near the absorption minimum of course is better, but some of the information in the complete spectrum is lost. Accordingly we must compromise in selecting the interval chosen for the analysis. A systematic analysis for the optimum interval is important, but it would constitute a major undertaking. As yet we have had to content ourselves with the somewhat arbitrary choice of the regions within 10% of the dispersion wavenumber. Examination of figure 14 gives an idea of the reasonableness of this choice.

With the idea of applying this analysis to representative samples, we have obtained the spectra for films of lithium fluoride at temperatures from 100°K to 300°K. The isotopic composition of the sample

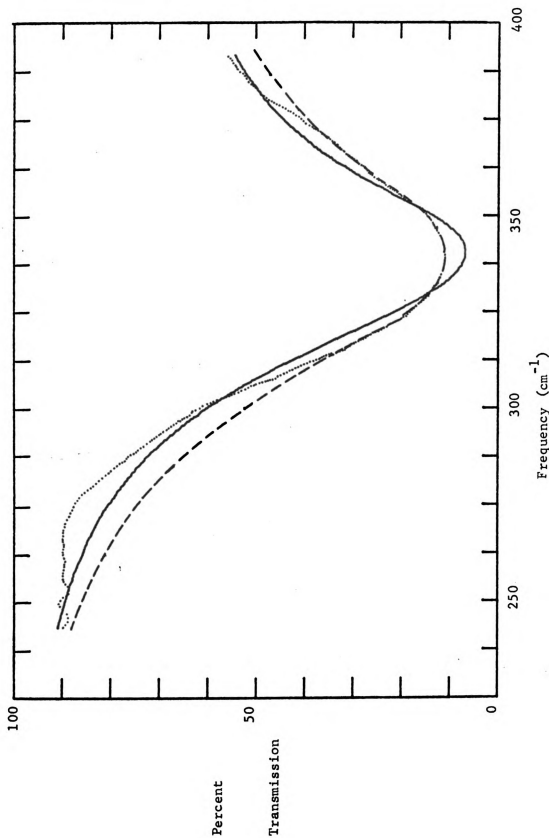


Figure 14. Absorption spectrum of a LiF film at 117°K (spectrum 174). The dotted line is the corrected experimental curve. The solid line is the calculated dispersion-oscillator fit when the entire curve is used as input for the nonlinear least-squares analysis. The resulting parameters are $d = 0.218\mu$, $\omega_0 = 340.8 \text{ cm}^{-1}$, $\gamma/\omega_0 = 0.061$. The dashed line is the corresponding fit when only the region around ω_0 is used as input. The resulting parameters are $d = 0.245\mu$, $\omega_0 = 339.8 \text{ cm}^{-1}$, $\gamma/\omega_0 = 0.091$.

material was controlled to have nearly pure Li^6F , nearly a half-and-half mixture of Li^6F and Li^7F , and nearly pure Li^7F , corresponding respectively and precisely to the fractions $x = 0.007$, 0.514 , and 0.9999 in the expression $[(1 - x) \text{Li}^6 \cdot x \text{Li}^7] \text{F}^{19}$. For Li^7F , films of various thicknesses were studied, to permit examination of the validity of the assumptions made in applying electromagnetic theory in equation (2). The parameters determined by the least-squares fit outlined above to the portion of these spectra within $\pm 10\%$ of ω_0 are listed in Appendixes A, B, C, and D respectively.

A direct investigation of whether the dispersion-oscillator formula fits the data better than some other kind of expression is sterile until the formula has been proved inadequate, or until a physical basis has been put forward for another expression. Instead we vary the experimental conditions of temperature, film thickness, and isotopic mass, and see whether the behavior of the parameters ω_0 , γ/ω_0 , and d is consistent with expectation. Table II summarizes the relations to be considered. They will now be discussed in some detail.

Infrared dispersion frequency ω_0

Dependence on thickness. - The parameter ω_0 is closely related to ω_{\min} , the frequency of minimum transmission, and is commonly taken as that frequency. Actually, on the dispersion-oscillator model, ω_{\min} varies slightly with thickness d for fixed ω_0 , as seen in figure 15, showing values of ω_{\min} calculated from equations (1) and (2) for LiF with ω_0 taken as 304 cm^{-1} and γ/ω_0 as 0.082 . Thus, although ω_{\min} may vary slightly with thickness, there is no reason for the parameter ω_0 as obtained in our analysis to vary with thickness, since it is characteristic of the material only.

At present we do not have facilities for direct measurement of the thickness, and we can determine only the apparent thickness; ω_0 should of course be just as independent of the apparent thickness d as the real thickness. Figure 16, a plot of ω_0 against d , shows that ω_0 is indeed constant at 306.0 cm^{-1} . To see whether this value is reasonable in view of our knowledge of other properties of the crystal, we make

Table II Expected dependence of single dispersion-oscillator parameters on experimental variables.

Experimental variables Derived parameter	Actual Thickness t	Isotopic Reduced mass \bar{M}	Temperature T
Dispersion frequency ω_0	t^0	$\bar{M}^{-1/2}$	$1 - aT$
Apparent thickness d	t^1	\bar{M}^0	T^0
Reduced damping constant γ/ω_0	t^0	Weakly Increasing	Increasing

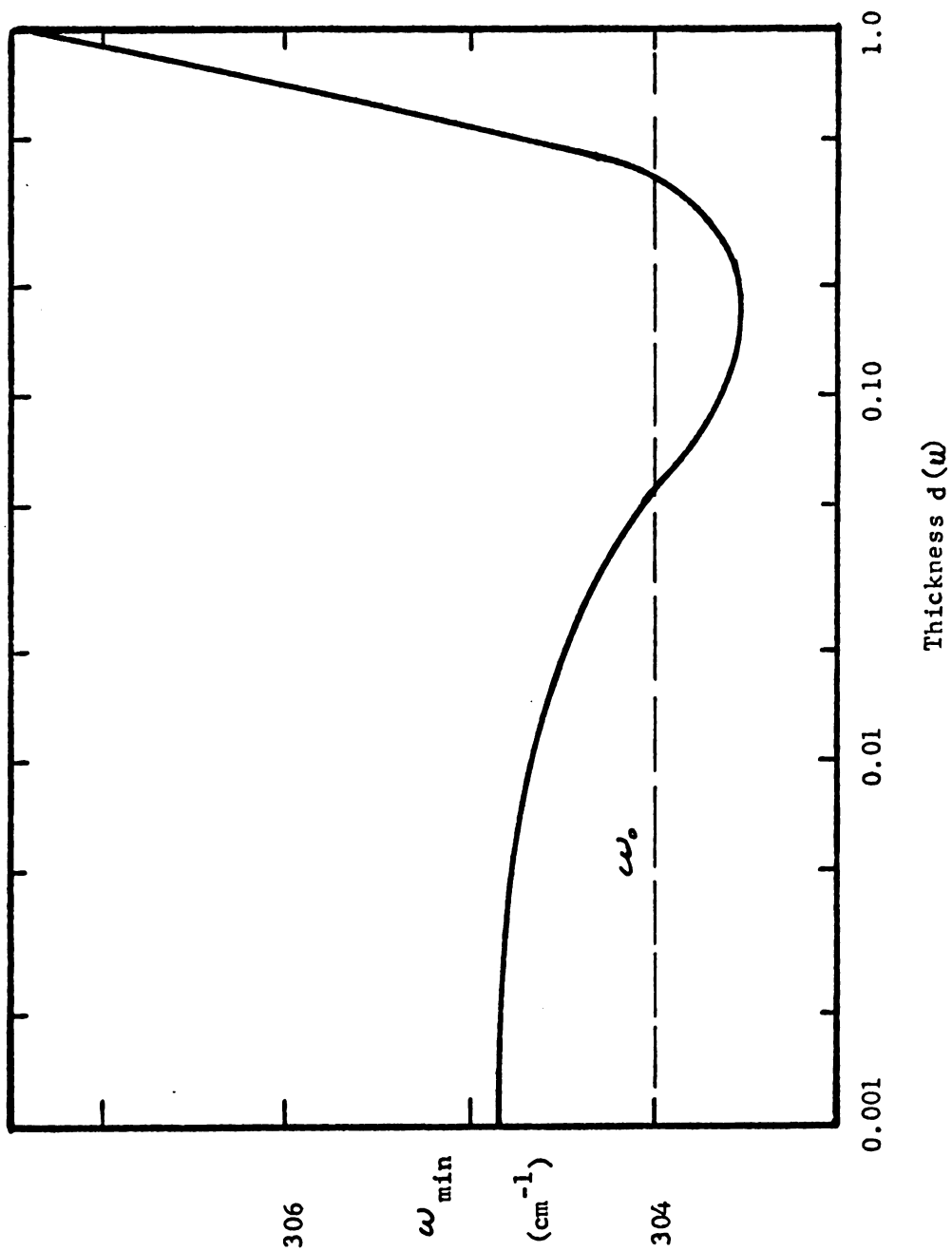


Figure 15. Dependence of ω_{\min} on thickness d as calculated from equations (1) and (2) for the dispersion oscillator model. Parameter values: $\omega_0 = 304.0 \text{ cm}^{-1}$, $\delta/\omega_0 = 0.082$.

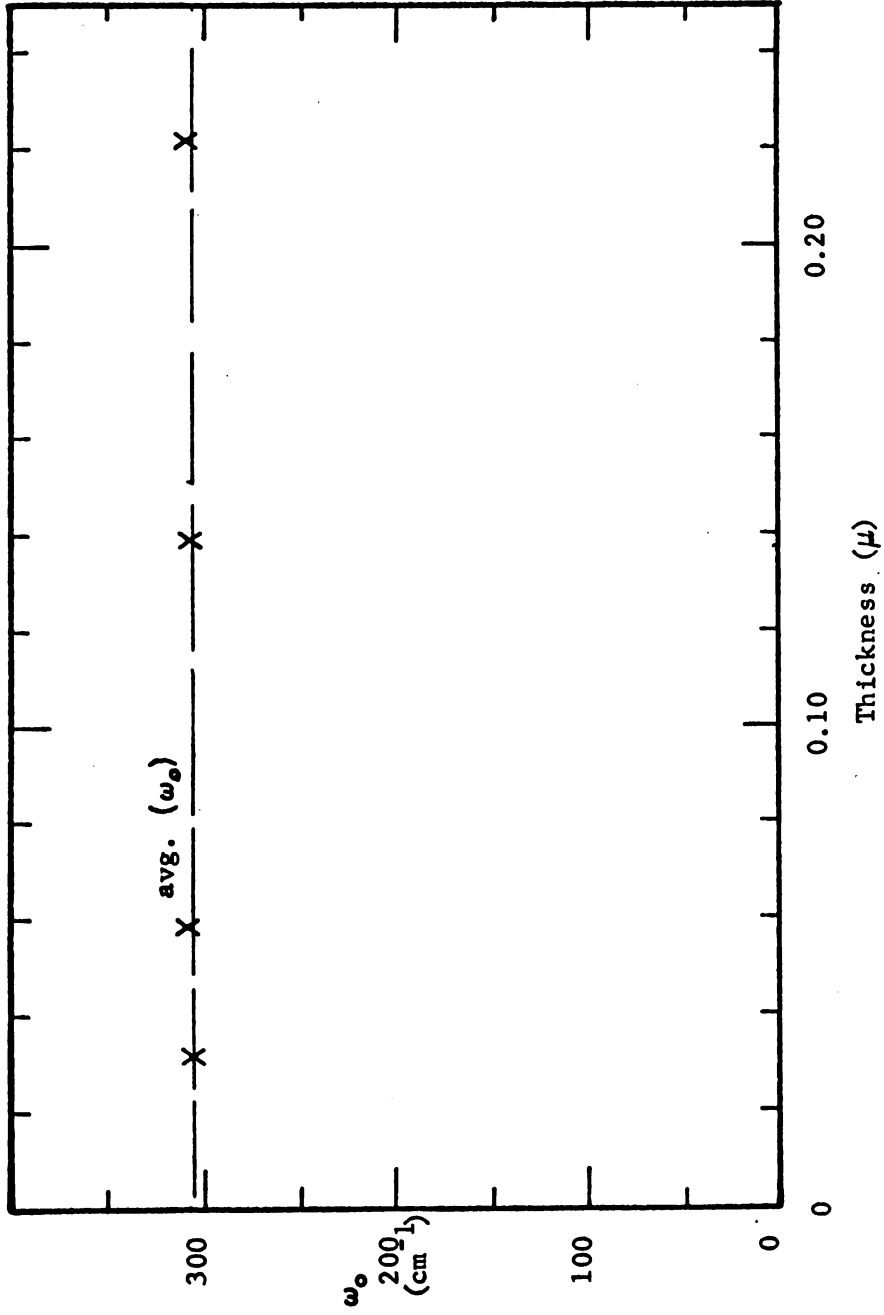


Figure 16. Dependence of ω_0 on apparent thickness d for a series of Li^7F films of various thicknesses.

use of Szigeti's relation¹⁷:

$$\omega_0^2 = [(\epsilon_\infty + 2)/(\epsilon_0 + 2)](6a/\bar{M}\beta), \quad (7)$$

where a is the lattice constant, \bar{M} is the reduced mass, and β is the compressibility. With room-temperature values of lattice constant¹⁸ $a = 1.98 \times 10^{-8}$ cm, compressibility¹⁹ $\beta = 1.35 \times 10^{-12}$ cm²/dyne, dielectric constants as given before, and with reduced mass $\bar{M} = 8.50 \times 10^{-24}$ gm, we find a calculated ω_0 of 319 cm⁻¹, in what is undoubtedly fortuitously close agreement with our room-temperature value of 306.0 cm⁻¹.

Dependence on isotopic mass. - A change in isotopic mass for a monatomic isotopically pure substance is equivalent to a change in the time scale for the motion in both classical and quantum mechanics, as follows directly from the equations of motion. That is, frequency may be traded for square root of reciprocal of mass, provided comparison is made at temperatures equivalent in the statistical-mechanics sense. For diatomic substances the relations are more complicated, but semi-quantitatively we should expect the same kind of behavior. We should perhaps then examine the ratio of $\omega_0(\text{Li-6})/\omega_0(\text{Li-7})$ at equal Debye temperatures; but, as will be seen, ω_0 varies only slightly with temperature, and it may seem less arbitrary to compare the values for different isotopic mass at the same temperature. At 300°K we find the observed ratio to be 324.7/306.0 = 1.0611, in good agreement with the reciprocal of the square root of the ratio of the reduced masses, 1.0590. This result is in good agreement with work done earlier by different methods by others in our laboratory²⁰. If we had compared the dispersion frequencies at equal Debye temperatures, that is, 300°K/1.059 = 283°K for Li⁷F corresponding to 300°K for Li⁶F, we would have found $\omega_0(\text{Li-6})/\omega_0(\text{Li-7}) = 1.0654$ (see figure 17). The difference is not important.

Dependence on temperature. - The effect of temperature T on ω_0 may be roughly estimated by the Szigeti relation (7), which should reflect the predictions of a more accurate theory. We compute from equation (7) the relation:

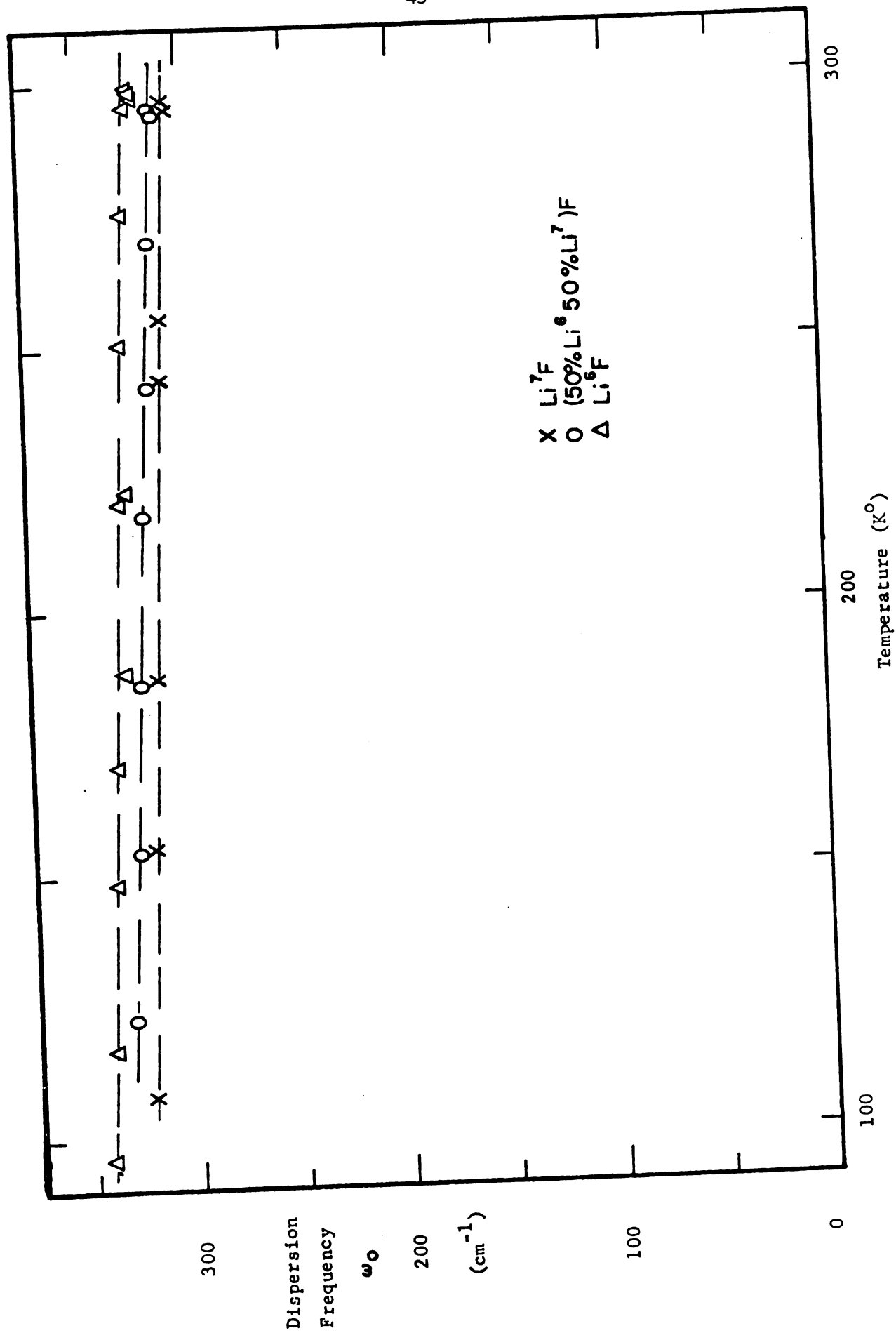


Figure 17. Dispersion frequency ω_0 versus temperature T for films of different isotopic composition.

$$\frac{1}{\omega_0} \frac{\partial \omega_0}{\partial T} = \frac{1}{2} \left[\frac{1}{a} \frac{\partial a}{\partial T} - \frac{1}{\beta} \frac{\partial \beta}{\partial T} - \frac{1}{(\epsilon_0 + 2)} \frac{\partial \epsilon_0}{\partial T} + \frac{1}{(\epsilon_{\infty} + 2)} \frac{\partial \epsilon_{\infty}}{\partial T} \right] \quad (8)$$

and list the contributions of the various terms, in Table III. By far the largest contribution is that due to the effect of thermal expansion on the static dielectric constant ϵ_0 . The overall effect is that $(1/\omega_0) \partial \omega_0 / \partial T = -142 \times 10^{-6}/\text{deg-K}$. The values observed for Li^6F and Li^7F in units of $10^{-6}/\text{deg-K}$ are respectively 255 and 239. This agreement is reasonable, considering the fact that all the temperature coefficients are room-temperature values.

Apparent thickness d

In contrast to ω_0 and γ/ω_0 , the parameter d is supposed to be characteristic of the particular films, and not of the material. In conjunction with the reduced damping constant γ/ω_0 , it determines the depth of the minimum.

Dependence on temperature. - Since thermal expansion causes a negligible change in actual film thickness (of the order of $200^\circ \times 50 \times 10^{-6}/\text{deg} = 1\%$), we should expect the apparent film thickness d to be nearly independent of temperature T. Figure 18, a plot of d against T, agrees with this prediction.

Dependence on actual thickness and isotopic mass. - We should of course expect the apparent thickness to equal the actual thickness as determined independently. As yet we have not developed techniques to measure the thickness directly. Until such measurements are made, we cannot verify that the apparent thickness is independent of actual thickness and isotopic mass, as the dispersion-oscillator model predicts.

Reduced damping constant γ/ω_0

Dependence on actual thickness. - Like ω_0 , the parameter γ/ω_0 is supposed to characterize the material only, and therefore be independent of thickness. In conjunction with the apparent thickness d, it determines the width of the absorption band. As explained before, we do not know

Table III Contribution of various terms to the dependence of the infrared dispersion frequency of LiF on temperature.

Source	Contribution $\times 10^6/K^0$	Reference
$\frac{1}{a} \frac{\partial a}{\partial T}$	+ 18	21
$\frac{1}{\rho} \frac{\partial \rho}{\partial T}$	- 12	19
$\frac{1}{\epsilon_0 + 2} \frac{\partial \epsilon_0}{\partial T}$	+ 306	15
$\frac{1}{\epsilon_\infty + 2} \frac{\partial \epsilon_\infty}{\partial T}$	- 9	16

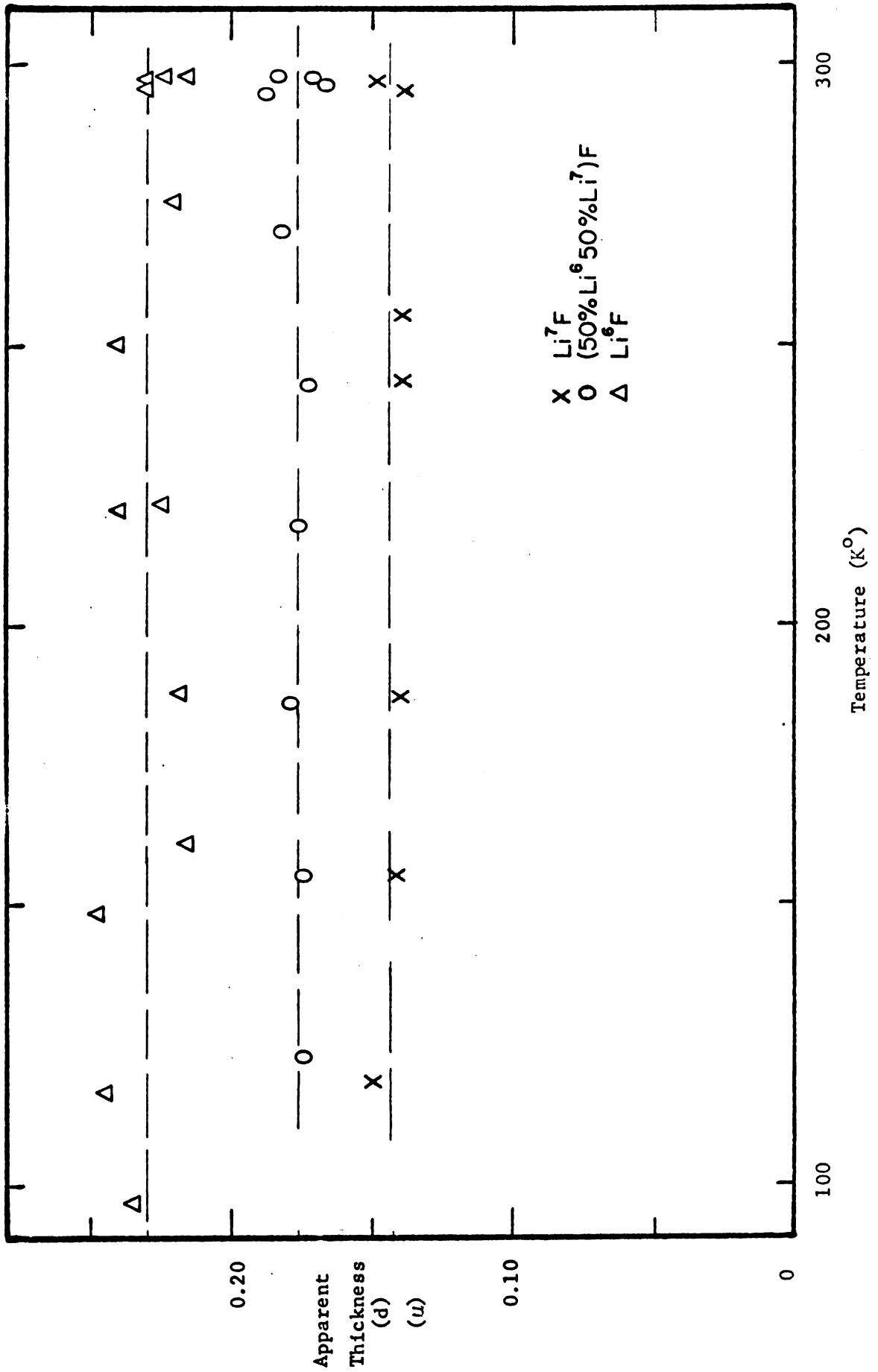


Figure 16. Apparent thickness d of three films of different isotopic composition versus absolute temperature, T .

the actual thickness t , and instead use the apparent thickness d as its measure. Figure 19, a plot of γ/ω_0 against d for the series of Li^7F films observed at room temperature, though it shows an unwelcome scattering, exhibits no trend. The agreement is probably acceptable.

Dependence on isotopic mass. - Here the theory is complicated, but isotopic mass can have only a slight effect. As an example, let us consider an expression derived by Born and Huang²²,

$$\gamma = \frac{2Chr_0^3 V^3}{\omega_0^4} \left(\frac{1}{M^2 m} + \frac{1}{m^2 M} \right) \left\{ 6 [\Psi''(r_0)]^2 + [2r_0^2 \Psi'''(r_0) + 3\Psi''(r_0)]^2 \right\} \quad (9)$$

where $\Psi(r_0^2)$ is the overlap energy function as a function of nearest-neighbor distance r_0 , V is the cell volume, C is a constant of the order of unity, M is the mass of the positive ion, and m is the mass of the negative ion. We compare damping at the same temperature, although perhaps we should choose equal Debye temperatures. Only M and ω_0 should change appreciably with isotopic mass. Hence we find the ratio of reduced damping constants should be

$$\frac{\gamma'/\omega_0'}{\gamma/\omega_0} = \left(\frac{M'}{M} \right)^{1/2} \left(\frac{m+M}{m+M'} \right)^{3/2}, \quad (10)$$

where the prime refers to Li^7F . For isotopically-pure lithium fluoride we find the value 1.018. Experimentally we observe too much scatter in γ/ω_0 to pick up a difference this small. We must content ourselves with noting that the reduced damping constants for both Li^6F and Li^7F lie in the same band on a plot of γ/ω_0 against T , as shown in figure 20 now to be discussed.

Dependence on temperature. - Although there exists no complete detailed theory of the broadening of absorption bands, the basic mechanism seems to be understood. In the harmonic approximation the absorption lines would be infinitely sharp; only mechanical anharmonicity and higher-order electric-dipole moments allow a broadening. At least two phonons must be involved, and these phonons can come from widely separated regions of the vibration spectrum. In any event, it seems

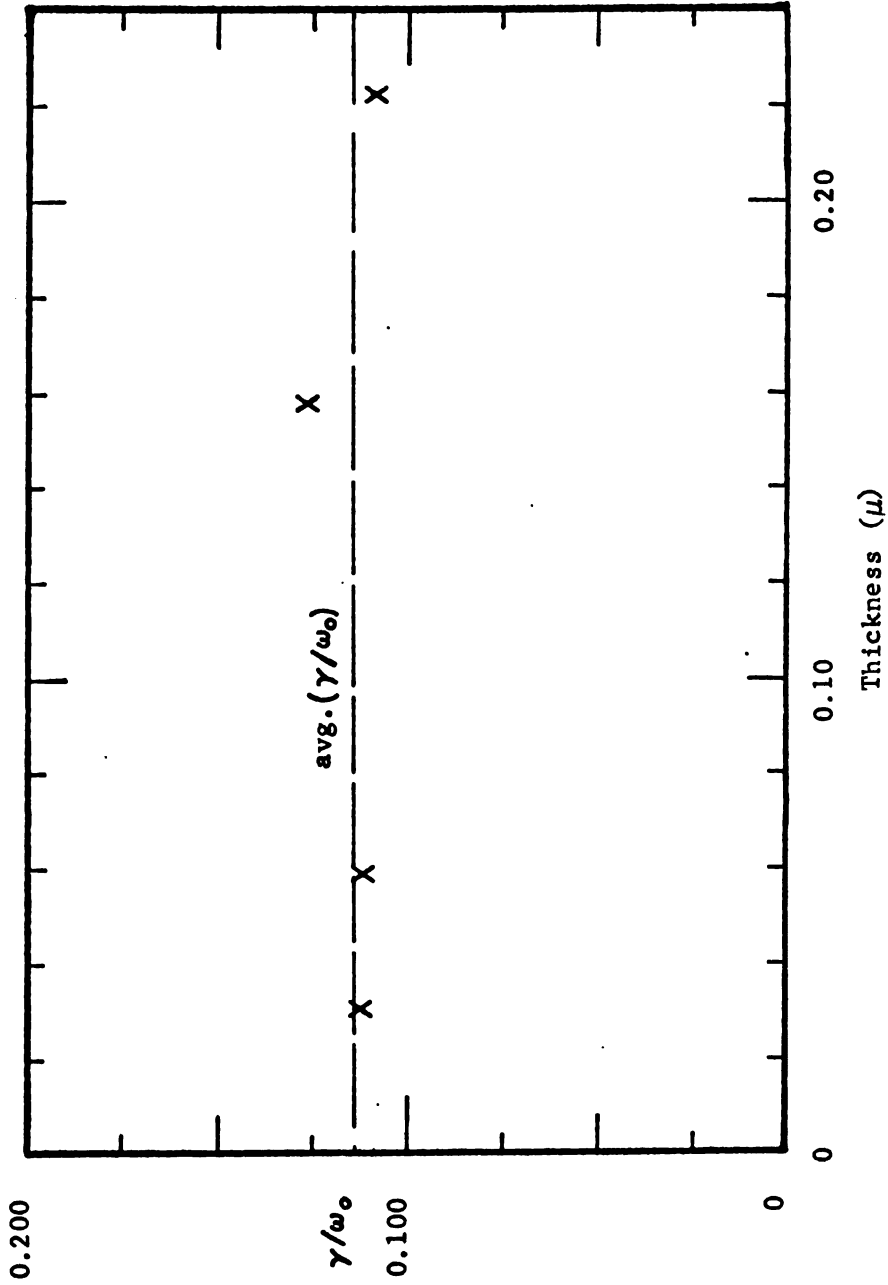


Figure 19. Reduced damping constant γ/ω_0 versus apparent thickness d for the several Li^7F films.

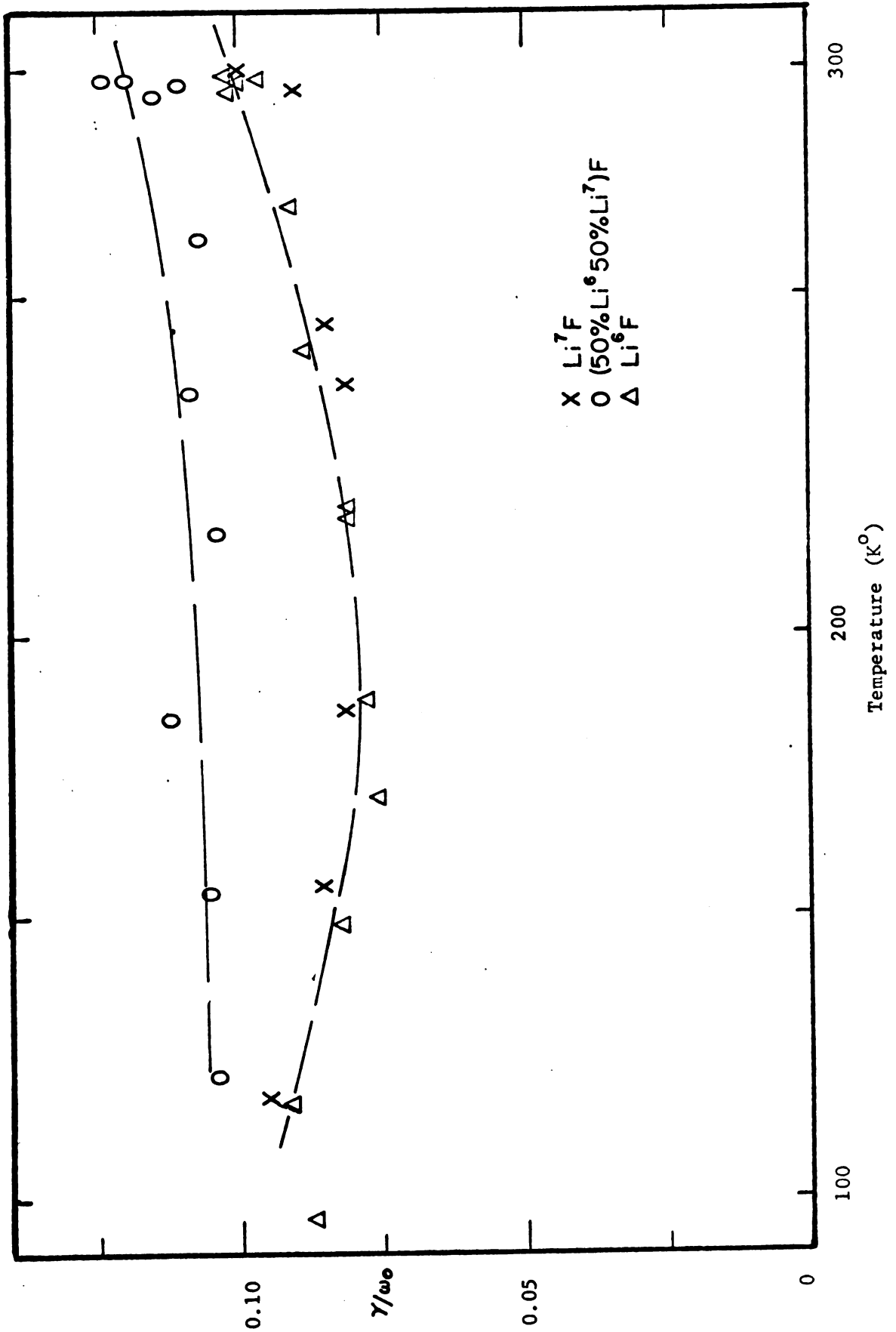


Figure 20. Reduced damping constant γ/ω_0 versus temperature T for films of different isotopic composition.

clear that at temperatures quite low in comparison with lattice characteristic temperatures, where virtually no phonons are present, the reduced damping γ/ω_0 should be nearly independent of temperature. As the temperature reaches values sufficient to excite appreciably the various peaks in the lattice-vibration spectrum, new absorption mechanisms enter, and the damping should increase.

Examination of the data exhibited in figure 20, plots of γ/ω_0 against T for films of various isotopic compositions, does little to confirm or refute this picture. The temperature where the reduced damping constant should start to rise can be estimated from the phonon spectrum. Figure 21, the spectrum calculated by Karo and Hardy²³, shows that few phonons will be excited thermally below about 200°K. Hence the damping should be constant below this temperature, and start to rise above it. Although a slight tendency for the curve to rise with increasing temperature may be read into the curve, it would be gratuitous to claim any real meaning until the low-temperature behavior can be explained. Apparently the damping starts to increase as the temperature falls below 120°K or so; there seems to be no way to understand this behavior theoretically, and it is likely that it is an artifact of the experimental technique or the analytical method. Until this point is resolved, we must keep in mind the limitations on the use of γ/ω_0 as a parameter to characterize the absorption.

Effect of Isotopic Mixing

We have deliberately excluded the dependence of the parameters on isotopic composition, because the theory is extraordinarily difficult. Rather our motivation is to use the parameters to characterize the effect of isotopic composition. Naively one might expect an isotopically-mixed crystal to behave like an isotopically-pure crystal of reduced mass equal to the average reduced mass of the mixture. For many properties this description is reasonable and correct. Let us test it for our parameters ω_0 , d, and γ/ω_0 , basing our comparison on our results for the 50%-50% mixture of Li⁶F and Li⁷F.

For the dispersion frequency, examination of figure 17 shows that ω_0 for the isotopically-mixed film is indeed intermediate between the values for the isotopically-pure films. At room temperature the

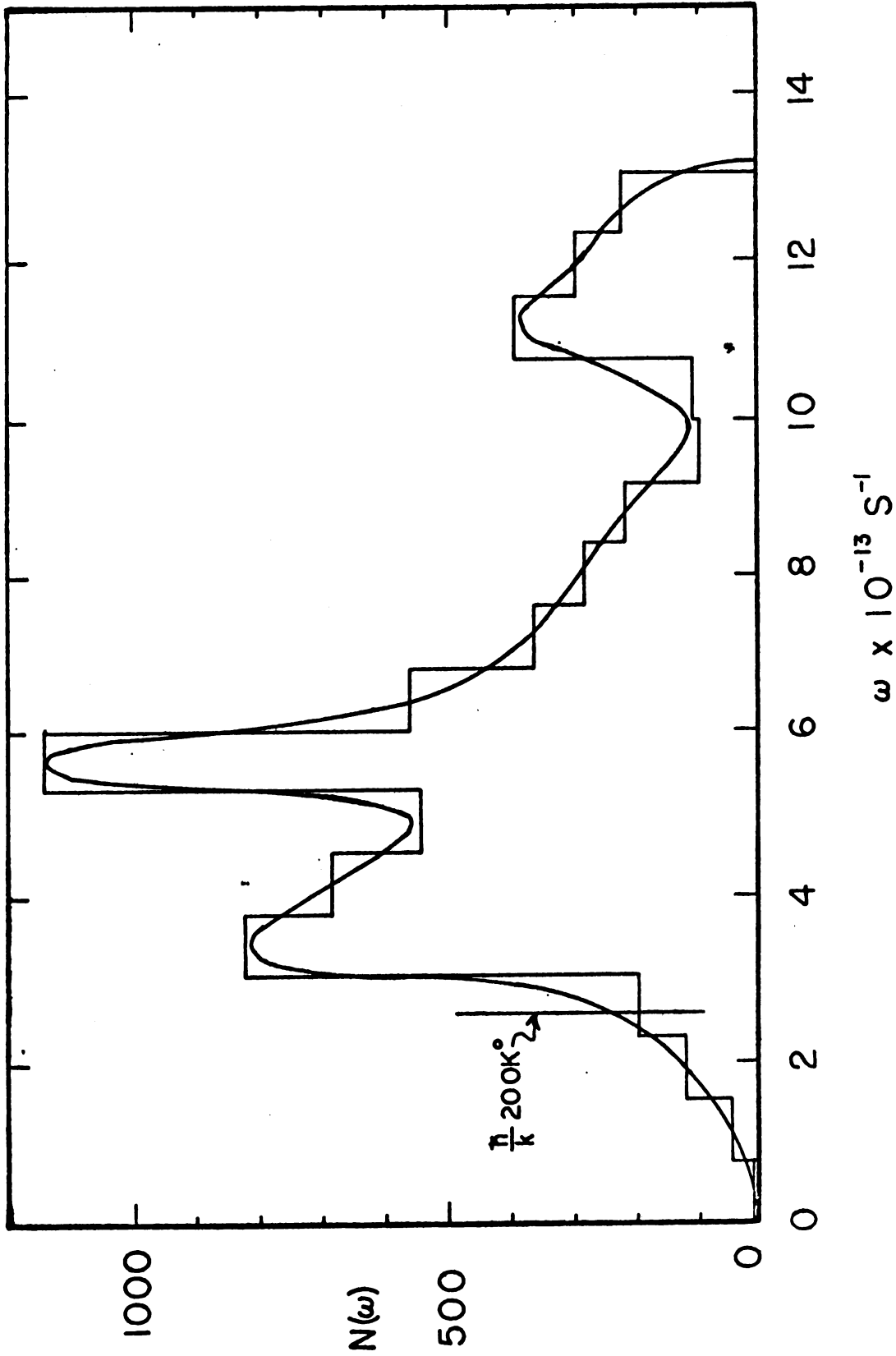


Figure 21. Phonon distribution function for LiF as calculated by Karo and Hardy²³.

observed ratios are: 1.033: 1.026: 1, those calculated as the reciprocals of the square root of the average reduced masses are 1.031: 1.027: 1. The agreement is satisfactory, and indeed continues to be so over the entire range of temperature given.

For the apparent thickness, there is little to add to the previous discussion for isotopically pure films; figure 18 shows the same kind of constancy of d with T .

For the reduced damping constant, we must surely give up our naive picture. The parameter γ/ω_0 is nearly independent of isotopic mass, on both theoretical and experimental grounds, as discussed above. Hence, for a given film thickness, the width of the absorption peak would be nearly independent of isotopic mass. Yet on another naive picture one might suspect the actual absorption in a mixed film might be something like a superposition of two separate absorption peaks, the components behaving more or less independently; the resultant peak would widen, and might even exhibit structure. In reality, of course, the lattice-vibration spectrum must be extremely complex in the case of mixed films, and the absorption peak must be something intermediate between the two naive models described. Examination of figure 20 shows the reduced damping constant to be significantly greater for the mixed film than for the pure film.

In sum, it appears that representation of the infrared dispersion peak by a Lorentzian oscillator permits a useful characterization of the optical behavior of films of ionic crystals in terms of two material parameters, ω_0 and γ/ω_0 , determined from absorption spectra of thin films, and two other material parameters ϵ_∞ and ϵ_0 , determined by other means. The behavior of these parameters with respect to temperature, isotopic composition, and (presumably) chemical composition should afford a valuable means of increasing our understanding of the interaction of electromagnetic radiation with crystals. Obviously other techniques, particularly reflection from thick single crystals, and Raman and Rayleigh scattering, are required to provide a basis for fuller understanding. But for studies of materials that are reactive, that are difficult to crystallize, or that are available only in small amounts, the study of absorption in thin films offers great promise.

The present work has demonstrated that it is practical to use a large portion of the absorption peak to determine the parameters, that the values thus obtained have considerable validity, and that the parameters behave about as reasonably as present theory is capable of predicting. Further experimental work must be carried out to increase the accuracy of the temperature measurements, and to develop methods of determining actual film thickness. Further work on the method of analysis must be carried out to establish the optimum portion of the spectrum to take for analysis, and to develop criteria of goodness of fit. Systematic investigation, then, of the effect of temperature and chemical composition in chemically and isotopically pure substances should lead to the elucidation of familiar phenomena; and investigation of the effect of chemical and isotopic composition in mixed crystals should lead to discovery of new phenomena.

REFERENCES

1. R. Bowling Barnes and M. Czerny, Z. Physik 72, 447 (1931);
R. Bowling Barnes, Z. Physik 75, 723 (1932).
2. G. K. White and S. B. Woods, Rev. Sci. Inst. 28, 638 (1957).
3. R. B. Belser, Rev. Sci. Inst. 25, 180 (1954).
4. Hanovia Liquid Bright Gold 261, Engelhard Industries, Inc.
5. H. J. Caswell, J. App. Phys. 32, 2641 (1961).
6. R. L. Powell, M. D. Bunch, and L. P. Caywood, Advances in Cryogenic Engineering 6, 537 (1960).
7. Henry Shenker, John I. Lauritzen, Robert J. Corruccini, and S. T. Lonberger, Reference Tables for Thermocouples, National Bureau of Standards Circular #561 (1955).
8. T. M. Dauphinee and S. B. Woods, Rev. Sci. Inst. 26, 693 (1955).
9. H. M. Randall, D. M. Dennison, Nathan Ginsburg, and Louis R. Weber, Phys. Rev. 52, 160 (1937).
10. K. N. Rao, R. V. DeVore, E. K. Plyler, J. Research National Bureau of Standards 67A, 351 (1963).
11. M. Born and K. Huang, Dynamic Theory of Crystal Lattices (Clarendon Press, Oxford, England, 1956), p. 83.
12. D. J. Montgomery and K. F. Yeung, J. Chem. Phys. 37, 1056 (1962).
13. M. H. Lietzke, "A Generalized Least Squares Program for the IBM 7090 Computer" ORNL-3259, available from the Office of Technical Services, Department of Commerce, Washington 25, D. C. (50¢).
14. M. Born and K. Huang, op. cit., p. 85.
15. J. S. Bosman and E. E. Havinga, Phys. Rev. 129, 1593 (1963).
16. R. S. Krishnan, Progress in Crystal Physics 1, 153 (1958).
17. B. Szigeti, Proc. Roy. Soc. A204, 51 (1950).
18. M. Born and K. Huang, op. cit., p. 52.
19. International Critical Tables (McGraw Hill, New York, 1928), Volume III, pp. 47, 48.
20. D. J. Montgomery and R. H. Misho, Nature 183, 103 (1959);
R. H. Misho, Ph.D. dissertation, Michigan State University, 1961.

21. Values of the coefficient of thermal expansion are taken from American Institute of Physics Handbook, Dwight E. Gray, editor (McGraw-Hill, New York, 1963), second edition, p. 4-73.
22. M. Born and K. Huang, op. cit., p. 362.
23. A. M. Karo and J. R. Hardy, Phys. Rev. 129, 2024 (1963).

APPENDIXES

Appendix A Infrared parameters of a $\text{LiF}^{6,19}$ film at various temperatures as determined by nonlinear least-squares analysis of that portion of the spectrum within $\pm 10\%$ of ω_0 .

Spectrum number	Temperature (K ^o)	Thickness d (microns)	Dispersion Frequency ω_0 (cm ⁻¹)	Reduced Damping Factor γ/ω_0
168	297.0	0.216	323.6	0.102
169	298.0	0.231	323.8	0.100
170	96.8	0.236	341.4	0.087
171	148.4	0.247	337.6	0.082
172	220.6	0.241	332.1	0.081
173	296.3	0.230	325.7	0.102
174	117.0	0.245	339.8	0.091
175	160.6	0.215	334.6	0.076
176	188.4	0.219	332.3	0.078
177	222.8	0.225	329.5	0.081
178	250.6	0.241	328.3	0.089
179	275.6	0.222	326.5	0.091
180	298.6	0.225	325.6	0.096

Appendix B Infrared parameters of a $[(51.37\%) \text{Li}^7, (48.63\%) \text{Li}^6] \text{Li}^6 \text{F}^{19}$ film at various temperatures, as determined by nonlinear least-squares analysis of that portion of the spectrum within $\pm 10\%$ of ω_0 .

Spectrum number	Temperature (K ^o)	Thickness d (microns)	Dispersion Frequency ω_0 (cm ⁻¹)	Reduced Damping Factor γ/ω_0
194	296	0.167	314.3	0.110
195	123	0.174	330.0	0.104
196	155	0.174	326.1	0.105
198	186	0.178	323.4	0.112
199	218	0.176	320.5	0.104
200	243	0.171	317.9	0.109
201	270	0.182	315.8	0.107
202	295	0.188	314.6	0.115
203	298	0.171	315.1	0.120
204	298	0.183	315.3	0.124

Appendix C Infrared parameters of a $\text{LiF}^{7,19}$ film at various temperatures as determined by nonlinear least-squares analysis of that portion of the spectrum within $\pm 10\%$ of ω_0 .

Spectrum number	Temperature (K°)	Thickness d (microns)	Dispersion Frequency ω_0 (cm^{-1})	Reduced Damping Factor γ/ω_0
184	118	0.149	321.7	0.095
185	155	0.141	317.8	0.085
186	187	0.139	315.1	0.081
188	244	0.139	309.9	0.081
189	255	0.139	307.8	0.085
190	296	0.138	306.2	0.090
191	297	0.150	305.4	0.998

Appendix D Room-temperature infrared parameters for a series of $\text{Li}^{7}\text{F}^{19}$ films as determined by nonlinear least-squares analysis of the spectrum within $\pm 10\%$ of ω_0 .

Spectrum number	Thickness d (microns)	Dispersion Frequency ω_0 (cm^{-1})	Reduced Damping Factor γ/ω_0
220	0.031	304.5	0.111
219	0.059	305.3	0.111
222	0.139	306.7	0.125
223	0.222	306.9	0.108

MICHIGAN STATE UNIV. LIBRARIES



31293017430178